Intestinal epithelial damage-derived mtDNA activates STING-IL12 axis in dendritic cells to promote colitis

Yajie Cai[a,#], Shuo Li[a,#], Yang Yang[a], Shuni Duan[a], Guifang Fan[a], Jinzhao Bai[a], Qi Zheng[a], Yiqing Gu[a], Xiaojiaoyang Li[b], Runping Liu[a,*]

[a] School of Chinese Materia Medica, Beijing University of Chinese Medicine, 11 Bei San Huan Dong Lu, Beijing, 100029, China

[b] School of Life Sciences, Beijing University of Chinese Medicine, 11 Bei San Huan Dong Lu, Beijing, 100029, China

***Corresponding author.** Runping Liu, Ph.D., School of Chinese Materia Medica, Beijing University of Chinese Medicine, 11 Bei San Huan Dong Road, 100029, Beijing, China, Email: liurunping@bucm.edu.cn, Tel: +86-10-53912122.

#These authors contributed equally to this work.

Abstract

Rationale: The treatment of ulcerative colitis (UC) presents an ongoing clinical challenge. Emerging research has implicated that the cGAS-STING pathway promotes the progression of UC, but conflicting results have hindered the development of STING as a therapeutic target. In the current study, we aim to comprehensively elucidate the origins, downstream signaling and pathogenic roles of myeloid STING in colitis and colitis-associated carcinoma (CAC).

Methods: *Tmem173*$^{fl/fl}$*Lzym-Cre*^{ert2} mice were constructed for inducible myeloid-specific deletion of STING. RNA-sequencing, flow cytometry, and multiplex immunohistochemistry were employed to investigate immune responses in DSS-induced colitis or AOM/DSS-induced carcinogenesis. Colonic organoids, primary bone marrow derived macrophages and dendritic cells, and splenic T cells were used for *in vitro* studies.

Results: We observed that myeloid STING knockout in adult mice inhibited macrophage maturation, reduced DC cell activation, and suppressed pro-inflammatory Th1 and Th17 cells, thereby protecting against both acute and chronic colitis and CAC. However, myeloid STING deletion in neonatal or tumor-present mice exhibited impaired immune tolerance and anti-tumor immunity. Furthermore, we found that TFAM-associated mtDNA released from damaged colonic organoids, rather than bacterial products, activates STING in dendritic cells in an extracellular vesicle-independent yet endocytosis-dependent manner. Both IRF3 and NF-κB are required for STING-mediated expression of IL-12 family cytokines, promoting Th1 and Th17 differentiation and contributing to excessive inflammation in colitis.

Conclusions: Detection of the TFAM-mtDNA complex from damaged intestinal epithelium by myeloid STING exacerbates colitis through IL-12 cytokines, providing new evidence to support the development of STING as a therapeutic target for UC and CAC.

Key Words: myeloid STING; dendritic cells; IL-12; mtDNA

Graphical abstract

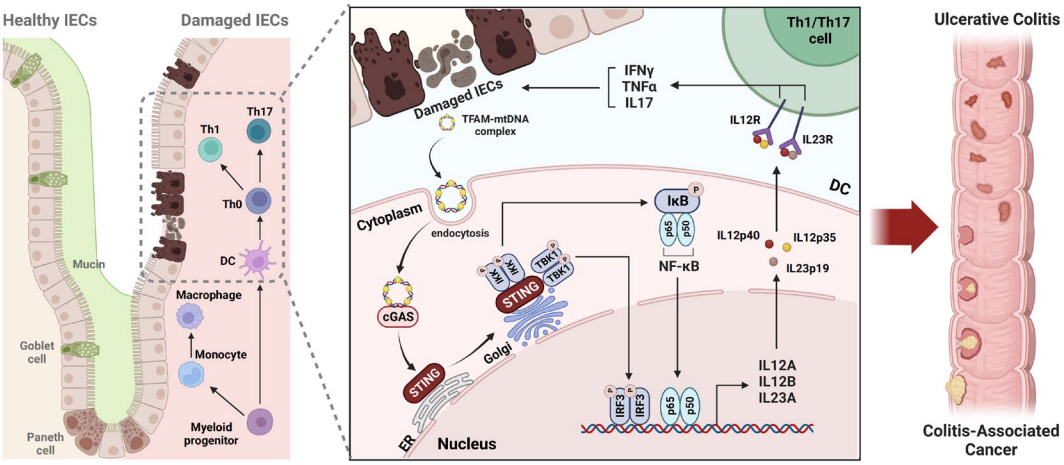

TFAM-associated mtDNA derived from damaged intestine epithelium triggered myeloid STING activation to induce IL-12 family cytokines, thus promoting Th1 and Th17 differentiation and contributing to excessive inflammation in colitis.

Introduction

Ulcerative colitis (UC) is a chronic inflammatory disease characterized by continuous and relapsing mucosal inflammation. Its incidence and prevalence have been rising around the world. Long-standing extensive UC is associated with increased risk of colorectal cancer (CRC), thus contributing to the mortality related to this disorder. However, the etiology and pathogenesis of UC remain poorly understood, and the unsatisfactory responses to current therapies pose significant challenges [1]. The abnormal activation of PRRs is closely related to multiple autoimmune diseases, including UC and colitis-associated cancer (CAC) [2]. Recently, stimulator of interferon genes (STING) pathway has emerged to be crucial mechanism in the development of UC by sensing foreign or self-origin dsDNA and promoting innate immune defense programs [3, 4]. The single-cell RNA-Sequencing data have shown that the expression of cGAS, STING, TBK1, IRF3, type I IFNs and interferon-stimulated genes (ISGs) were upregulated in active UC patients and in multiple colitis murine models [5, 6]. It was also reported that the deficiency of STING significantly alleviated intestinal inflammation in mice, while the inflammation was worsened after administration of STING agonist DMXAA [7, 8]. Besides, spontaneous chronic colitis and fibrosis occurred in mice with structural activation of STING (known as N153S mice). Myeloid-derived STING has further been recognized to play a vital role in mediating the development of colitis [6]. Specific knockout of STING in $Lysm^+$ cells and $CD11c^+$ cells were found to ameliorate AOM/DSS-induced CAC [7]. These data all suggest that the activation of STING pathway, especially STING stimulation in myeloid cells, may involve in the pathogenesis of UC.

However, Yang *et al.* recently found that abrogation of STING in $CD4^+$ T cell induced more severe colonic inflammation through increasing the proportion of pathogenic Th1 cell and suppressing the production of the anti-inflammatory IL-10 [9]. Another study discovered that congenital knockout STING significantly limited the growth of intestinal barrier and the maturation of local immune homeostasis, leading to immune intolerance and eventual aggravation of colitis [10]. Hence, the precise role

of STING in colitis remains a subject of debate, and comprehensive and systematic investigations on the function and mechanism of STING are necessary.

The triggers of STING activation and its downstream signaling in UC development is also a mystery. Zhao *et al.* suggested that nuclear DNA and mtDNA packaged by extracellular vesicles (EVs) leaked from damaged intestinal epithelial cells stimulated the STING pathway, thus triggering intestinal inflammation in murine colitis and active human CD [11]. However, another report suggested that commensal bacteria and its product c-di-GMP stabilize the expression of STING protein by enhancing K63-linked ubiquitination of STING [6]. In terms of STING-mediated signaling, it was demonstrated that myeloid-differentiation primary response protein (MyD88)-dependent IL-1β and IL-18 release exerted pro-inflammatory effects after STING stimulation [7]. The accumulation of Th1 effector cells was also proposed as the downstream immune responses upon STING activation, suggesting the involvement of adaptive immunity in the progression of STING-related colitis [6]. However, the interaction between myeloid-derived STING pathways and downstream adapt immune responses still lacks evidence.

In the current study, we established DSS-induced acute and chronic colitis models on neonatal and adult *Tmem173*$^{fl/fl}$*Lzym-Cre*^{ert2} mice, aiming to investigate the exact effects and immune mechanisms of cell-specific and time-dependent STING knockout on UC progression and AOM/DSS-induced CAC. Additionally, we utilized colonic organoids, BMDMs, BMDCs, and primary splenic T cells to elucidate the triggers, signaling transduction, and downstream effectors of STING activation in regulating native and adaptive immune responses during colitis.

Materials and methods

Animals

C57BL/6N, *Tmem173*$^{fl/fl}$ mice, and *Lzym-Cre*^{ert2} mice were purchased from Shanghai Model Organisms Center, Inc. (Shanghai, China). *Tmem173*$^{fl/fl}$ mice were crossed with *Lzym-Cre*^{ert2} mice to obtain *Tmem173*$^{fl/fl}$*Lzym-Cre*^{ert2} mice (referred as

Tmem173$^{i\Delta mye}$ mice). *Tmem173*$^{-/-}$ mice were kind gifts from Prof. Yao Wang at Beijing University of Chinese Medicine. All genetically modified mice were on the C57BL/6N background. All animal studies were conducted in accordance with the guidelines approved by the Institutional Animal Care and Use Committee at Beijing University of Chinese Medicine guidelines (BUCM-4-2022012001-1096).

Tamoxifen-induced myeloid-specific deletion of *Tmem173*

To achieve conditional knockout of *Tmem173* in the myeloid cells of mice, 5 to 6-week-old or 6 to 8-week-old *Tmem173*$^{fl/fl}$ mice and *Tmem173*$^{fl/fl}$*Lzym-Cre*^{ert2} mice were injected intraperitoneally with 120 mg/kg tamoxifen (TAM; ADAMAS, Basel, Switzerland) dissolved in corn oil every other day for 5 times. In the chronic DSS colitis model and AOM/DSS-P groups, we maintained TAM induction twice a week to ensure long-term myeloid-specific STING knockout during the experiments. Neonatal *Tmem173*$^{fl/fl}$ mice and *Tmem173*$^{i\Delta mye}$ mice were injected with the same dose of TAM into the stomach for 5 continuous days. Genotyping was performed when the mice were four-week-old, following the guidance of Direct Mouse Genotyping Kit (APExBIO, Houston, USA).

Acute and chronic DSS colitis

C57BL/6N mice, *Tmem173*$^{-/-}$ mice, *Tmem173*$^{fl/fl}$ mice, and *Tmem173*$^{i\Delta mye}$ mice at the age of 6 to 8-week-old were administered with 2.5%-3% (w/v) dextran sodium sulfate (DSS; MP Biomedicals, California, USA) dissolved in the drinking water for 7 days followed by 1 day water. The control group mice were received regular distilled water. The body weight of mice was monitored every day. Colon tissue was harvested, disease activity index was evaluated, and spleen coefficient (spleen weight divided by the body weight) was calculated at the end of the experiment.

After given one-week acute DSS induction, 6 to 8-week-old *Tmem173*$^{fl/fl}$ mice and *Tmem173*$^{i\Delta mye}$ mice were administered with a cycle of three days of normal drinking water followed by four days of 2.5%-3% DSS, and this cycle was repeated for three times. The body weight of mice was monitored every day. Colon tissue was harvested, disease activity index was evaluated, and spleen coefficient was calculated at the end

of the experiment.

The extraction of colonic lamina propria cells

The extraction of colonic lamina propria cells was performed under the guidance of lamina propria dissociation kit (Miltenyi, Bergisch Gladbach, Germany). The colonic samples were isolated, flushed, and then cut into 2 to 4 mm fragments. The colonic samples were transferred into 1× HBSS solution containing 5 mM EDTA, 5% fetal bovine serum (FBS) and 1 mM DTT for 20 min at 37 °C under rotation of 12 rpm to remove colonic epithelial cells. This pre-digestion process was repeated twice. Remaining colonic samples was digested by pre-heated 1× HBSS solution containing 5% FBS with mixed enzyme on the gentleMACS Dissociator (Miltenyi, Bergisch Gladbach, Germany). The cell suspension was filtered through 100 μm strainer and then centrifuged at 300×g for 10 min. The cell viability of isolated lamina propria lymphocytes was analyzed by AO/PI dye (Counterstar, Shanghai, China) and was over 80%, which was enough to for further applications.

The isolation and culture of colonic organoids

The colonic samples were isolated, flushed, and then cut into 2 to 4 mm fragments. Then the colonic fragments were washed by PBS containing 10% FBS (washing solution) till the supernatant was clear. The colonic samples were incubated with 2 mM EDTA for 15 min at 4 °C to digest the colonic crypts, and were then washed by washing solution. This process was repeated twice. The suspension was filtered through a 70 μm strainer and the filtered crypts were collected. The crypts were resuspended with Matrigel and added into 24 well plates at 37 °C for 5-10 min till the Matrigel was solidified, the BM2 medium containing 50 ng/μL EGF, 100 ng/μL Noggin, and 1 μg/μL R-Spondin-1 (culture solution) was added in each well. The fresh culture solution was replaced 2 to 3 times. The colonic organoids needed to be passaged by DMEM/F12 medium containing 1% GlutaMax and 1% HEPES when they became bigger. The organoids were treated with 100 ng/mL TNF-α to induce apoptosis, and the supernatant was collected 2 h later. PI staining was performed to evaluated the injury of colonic organoids.

The isolation of DNA from the conditioned medium of colonic organoids

DNA isolation from the cultured medium of colonic organoids was performed under the guidance of QIAamp Blood DNA mini kit (QIAGEN, Dusseldorf, Germany). The quality examination and quantification of isolated DNA were performed using Nanodrop (Thermo Scientific, Madison, USA), and then the concentration of DNA in CM was calculated.

The measurement of mtDNA

Real-time qPCR was employed for the quantification of mtDNA and nuclear DNA using specific primers for mitochondrial genes, including mt-12S1, mt-CO3, mt-CytB, and the nuclear gene rn18S, and results were normalized with rn18S.

DNA uptake in BMDCs

DNA uptake of BMDCs was measured by DRAQ5 Fluorescent Probe (Thermo, Massachusetts, USA). The supernatant of isolated colonic organoids treated with or without TNF-α was collected and incubated with 5 μM DARQ5 Fluorescent Probe and 10 mM HEPES for 115 min at 37 °C. WT BMDCs were incubated with the DRAQ5-stained conditional medium for 6h and subjected to flow cytometry.

Immunoprecipitation (IP) of TFAM-associated mtDNA

Protein A/G beads were incubated with IgG and anti-TFAM antibodies overnight at 4 °C with rotator to obtain IgG antibody-coated beads and anti-TFAM antibody-coated beads. Then blank Protein A/G beads with the supernatant of colonic organoids were mixed for 30 min at 4 °C with rotator to block the samples. After centrifugation, the blocked samples were transferred into IgG antibody-coated beads and anti-TFAM antibody-coated beads and then rotated overnight at 4 °C. The obtained precipitate and supernatant were utilized for *in vitro* studies and DNA isolation.

Quantification and statistical analysis

All values expressed as mean ± SEM were statistically analyzed using GraphPad Prism (version 8.0). Differences among group means were determined with one-way ANOVA with a Tukey *post hoc* test for multi-group comparisons, or an unpaired two-tailed Student's *t* test between two groups. P value of less than 0.05 was considered

statistically significant.

Results

Myeloid-specific knockout of STING in adult mice ameliorates DSS-induced acute and chronic colitis.

To define the role of STING pathway in the development of colitis, we utilized C57BL/6N mice to establish DSS-induced acute and chronic colitis models **(Figure S1A and D)**. The phosphorylation of STING and activation of downstream transcription factors, including interferon regulatory factor 3 (IRF3), nuclear factor kappa-B (NF-κB), and IRF7, were all significantly elevated in colitis **(Figure S1B, C, E and F)**. Our results further suggested that global knockout (KO) of STING remarkably inhibited the expression of inflammatory genes and ameliorated colitis, which support the findings of Shmuel-Galia *et.al* [6] but not Yang *et.al* [9] **(Figure S1G-N)**. Since myeloid cell-mediated innate immunity is a master regulator in colitis, we established a tamoxifen (TAM) inducible CreERT2 dependent and myeloid cell-specific STING KO mice (*Tmem173*$^{i\Delta mye}$) to explore the exact pathogenic role of STING activation. Five continuous times of TAM administration could significantly induce the deletion of STING in adult *Tmem173*$^{i\Delta mye}$ mice. As shown in **Figure 1A**-**B**, myeloid knockout of STING significantly relieved body weight loss, increased colon length (**Figure 1C-E**), decreased the disease activity index (DAI) score (**Figure 1D**), and reduced spleen coefficient (**Figure S2A**) in acute colitis. Histological analysis further revealed that intestinal epithelial injury, associated with lymphocyte infiltration and mucosal barrier impairment, were dramatically improved in *Tmem173*$^{i\Delta mye}$ mice when compared with litter-mate *Tmem173*$^{fl/fl}$ mice (**Figure 1F-G**). *Tmem173*$^{i\Delta mye}$ mice were also significantly protected from prolonged and repeated DSS-induced chronic colitis, as illustrated in **Figure 1H-L**, and **Figure S2B** and showed improved survival rate (**Figure S2C**). Histopathological evaluation further supported above findings (**Figure 1M-N**). From the perspective of cytokine expression, qPCR analysis demonstrated that the upregulation of *Il1b*, *Tnfa*, and *Il6* were diminished in *Tmem173*$^{i\Delta mye}$ mice in both acute and chronic

colitis (**Figure S2D-E**).

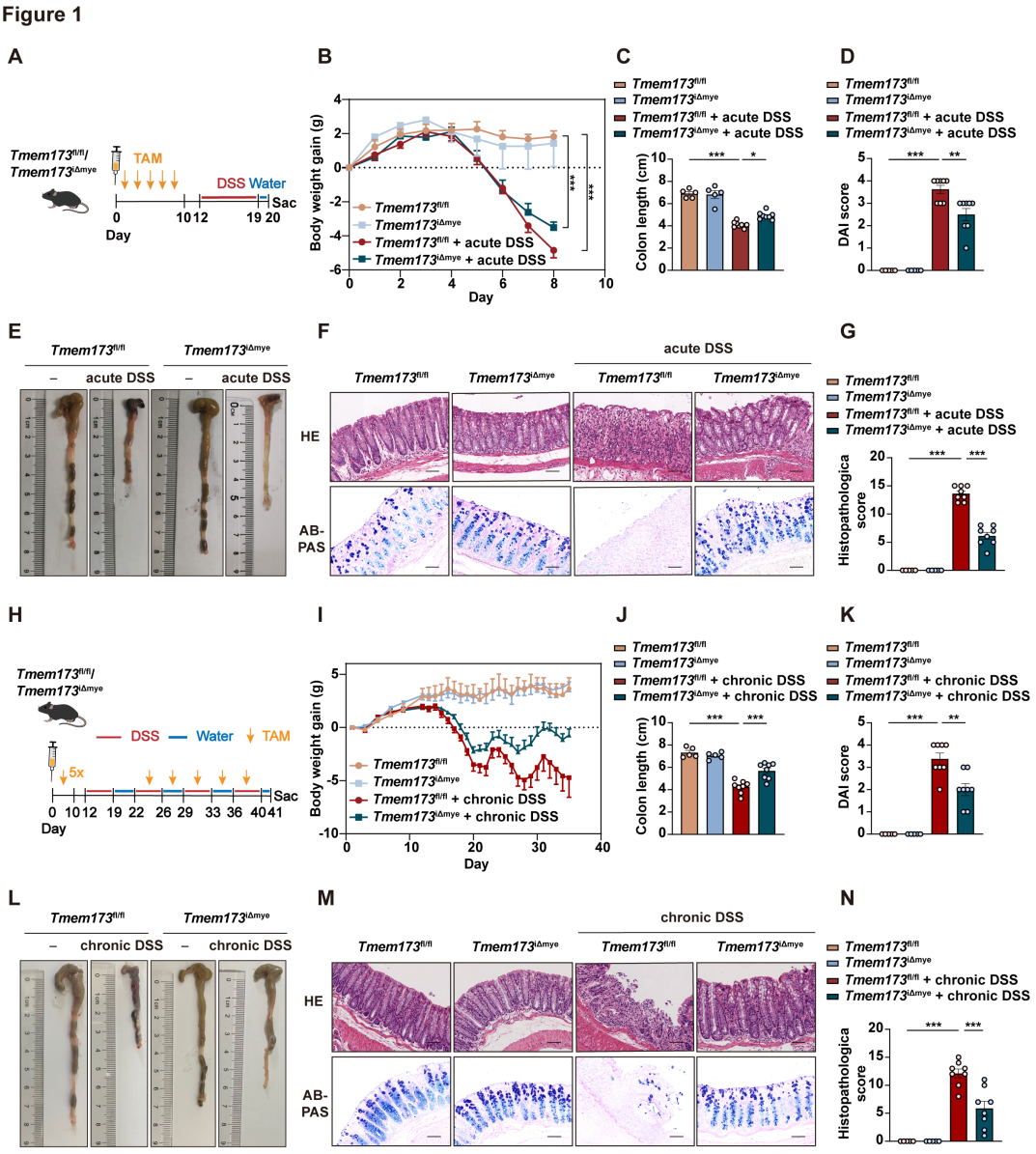

Figure 1. Myeloid-specific knockout of STING in adult mice ameliorates DSS-induced acute and chronic colitis. (A-G) *Tmem173*$^{fl/fl}$ mice and *Tmem173*$^{i\Delta mye}$ mice were induced by acute DSS colitis after tamoxifen (TAM) treatment. **(A)** Animal experimental design. **(B)** Body weight gain. **(C)** Colon length. **(D)** DAI score. **(E)** Representative colon pictures. **(F)** Representative H&E and AB-PAS staining of colonic sections. **(G)** Histopathological score. **(H-N)** *Tmem173*$^{fl/fl}$ mice and *Tmem173*$^{i\Delta mye}$ mice were induced by chronic DSS colitis after TAM treatment. **(H)** Animal experimental design. **(I)** Body weight gain. **(J)** Colon length. **(K)** DAI score. **(L)** Representative colon

pictures. **(M)** Representative H&E and AB-PAS staining of colonic sections. **(N)** Histopathological score. Scale bars, 100 μm. Values represent the mean ± S.E.M. of at least five mice in each group. Statistical significance: *p < 0.05, **p < 0.01, ***p < 0.001.

The myeloid-specific knockout, similar to the systemic knockout of STING, notably decreased the upregulation of STING in inflamed colon tissue (**Figure 2A**), suggesting that in the case of UC, the activation of the STING pathway is primarily in myeloid cells rather than other cell types like epithelial cells. **Figure 2B** further supported this hypothesis. While there is mild increase of STING expression in epithelial cells, a substantial number of infiltrating CD11b and STING double-positive cells are observed in UC (**Figure S2F-J**). In *Tmem173*$^{i\Delta mye}$ mice, the infiltration of CD11b^{+} cells significantly decreased, along with a specific loss of STING expression in CD11b^{+} cells, leading to an improvement in the structure of the colon barrier.

Previous studies have reported increased susceptibility to colitis in mice with congenital deletion of STING [10]. Hence, we are curious to investigate whether the neonatal deletion of myeloid STING actually aggravates colonic inflammation. TAM was intraperitoneally injected into newborn *Tmem173*$^{fl/fl}$ mice and *Tmem173*$^{fl/fl}$*Lzym-Cre*^{ert2} mice for continuous five days. The administration of DSS was carried out when these mice reached the age of 7 weeks (referred as N-*Tmem173*$^{fl/fl}$ + DSS group and N-*Tmem173*$^{i\Delta mye}$ + DSS group, respectively) (**Figure S3A**). Interestingly, N-*Tmem173*$^{i\Delta mye}$ mice exhibited greater body weight loss, colon shortening and disease severity in response to DSS treatment (**Figure S3B-E**). Histological analysis revealed more severe inflammatory infiltration and tissue damage (**Figure S3F-G**). The transcript levels of inflammatory genes, including *Tnfa*, *Il1b*, and *Il6,* were significantly higher in DSS-treated N-*Tmem173*$^{i\Delta mye}$ mice as well (**Figure S3H**). Contrary to the more severe colitis, there was a decrease in the infiltration of CD11b^{+} myeloid cells and a significant reduction in the expression of STING in the colon of N-*Tmem173*$^{i\Delta mye}$ mice (**Figure S3I**). This finding suggests that the absence of STING in neonatal mice

may disrupt the establishment of immune tolerance in the intestinal lamina propria, warranting further investigation.

Decreased myeloid-derived dendritic cells and diminished activation of Th1 and Th17 Cells are observed in colitic *Tmem173*$^{i\Delta mye}$ mice

To investigate the immunoregulatory mechanisms underlying the alleviation of colitis following myeloid-specific STING knockout, we performed RNA-seq analysis. Principal component analysis (PCA) revealed significant differences in the gene expression profile between colitic *Tmem173*$^{i\Delta mye}$ mice and *Tmem173*$^{fl/fl}$ mice (**Figure 2C**). A total of 2008 DEGs were commonly identified in both *Tmem173*$^{fl/fl}$ + DSS vs. *Tmem173*$^{fl/fl}$ and *Tmem173*$^{i\Delta mye}$ + DSS vs. *Tmem173*$^{fl/fl}$ + DSS (**Figure S4A**), which are highly likely to be associated with the protective effects of myeloid STING KO. Specifically, 176 downregulated DEGs, including *Cebpd*, *Cebpb*, *Ccl2,* and *Cxcl1*, and 133 upregulated DEGs, including *Sectm1b*, *Slc26a3*, *Fgd4,* and *Slc6a14, were found in Tmem173*$^{i\Delta mye}$ + DSS vs. *Tmem173*$^{fl/fl}$ + DSS (**Figure 2D**). GO, KEGG and GSEA analysis suggested that these DEGs are enriched in multiple inflammation-related pathways, such as myeloid leukocyte migration, differentiation, and cytokines production, acute inflammatory response, and T cell differentiation and activation involved in immune response (**Figure S4B** and **Figure 2E**). As depicted in **Figure 2F**, downregulation of acute phase response-related genes, such as *S100a8* and *S100a9*, and canonical pro-inflammatory cytokines and chemokines, such as *Il6*, *Il1b*, and *Ccl2,* was along with suppressed expression of genes contributes to leukocyte chemotaxis and activation like *Trem1*, *Cxcl10*, *Il12a*, thereby linking altered innate immunity to adaptive immunoregulation following myeloid STING KO.

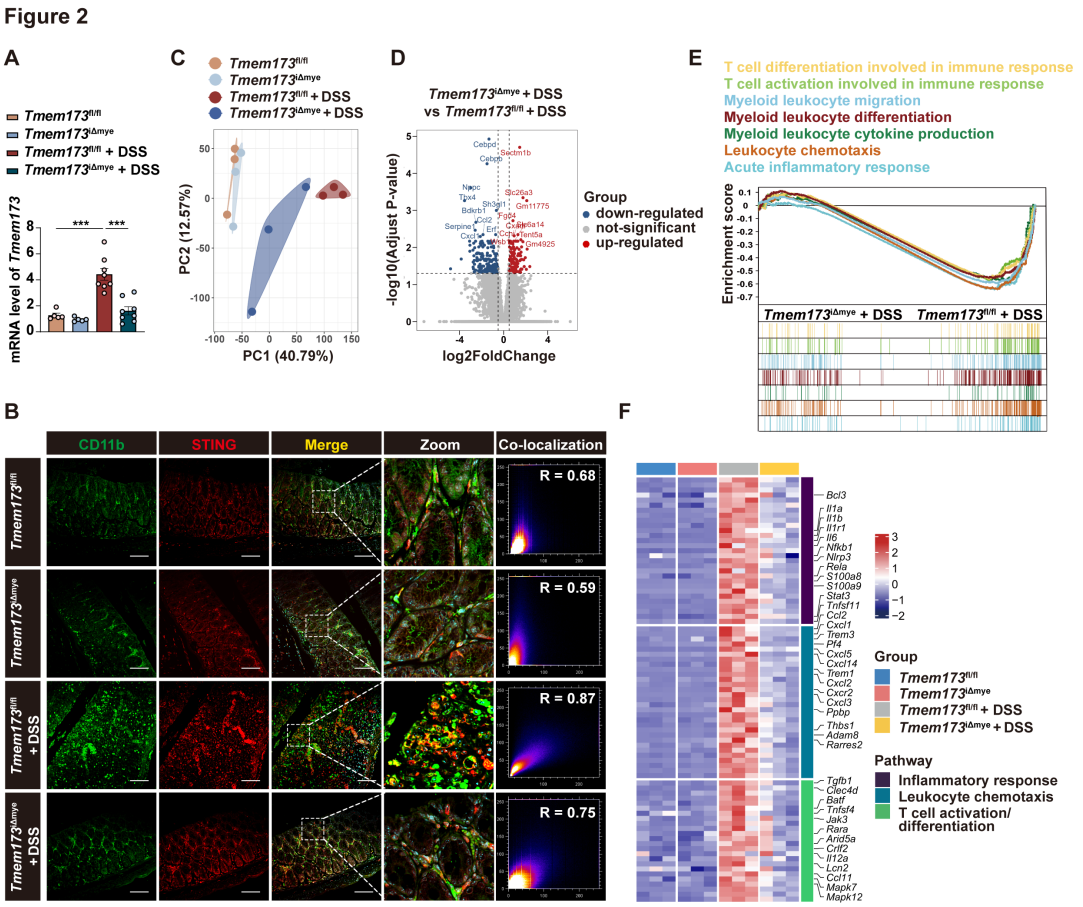

Figure 2. Effects of myeloid-specific knockout of STING on innate immunity and adaptive immunoregulation. (A) Relative mRNA levels of *Tmem173* in the colon. **(B)** Representative immunofluorescent co-staining of CD11b and STING of colonic sections. **(C)** The principal components analysis (PCA). **(D)** Volcano plot of DEGs in *Tmem173*$^{i\Delta mye}$ + DSS *vs* *Tmem173*$^{fl/fl}$ + DSS. Down-regulated genes are in blue and up-regulated genes are in red. The cutoff values |log2FoldChange| < 0.5 and adjusted p value < 0.05 were utilized to identify differentially expressed genes. **(E)** GSEA analysis on pathways related to innate and adaptive immune responses in *Tmem173*$^{i\Delta mye}$ + DSS *vs* *Tmem173*$^{fl/fl}$ + DSS. Scale bars, 100 μm. **(F)** DEGs in pathways related to inflammatory response, leukocyte chemotaxis and T cell activation/differentiation. Values represent the mean ± S.E.M. of at least five mice in each group. Statistical significance: ***p < 0.001.

To further investigate the potential connection between innate and adaptive

immunity, we utilized Cibersort to analyze the proportion of various immune cells based on RNA-seq data. (**Figure S5A-B**). Specifically, increased abundance of monocytes, immature DCs, activated DCs, M0 macrophage, Th1 and Th17 cells was observed in the colon from colitic *Tmem173*$^{fl/fl}$ mice, which was all decreased to a certain extent in *Tmem173*$^{i\Delta mye}$ mice (**Figure S5C**). We thus hypothesized that the absence of STING in myeloid cells alleviated intestinal inflammation by reducing DC and macrophage infiltration, and Th1 and Th17 cell differentiation. To test the hypothesis, we evaluated immune cell profiles in the lamina propria cells isolated from colon of colitic *Tmem173*$^{fl/fl}$ mice and colitic *Tmem173*$^{i\Delta mye}$ mice using flow cytometry. The immune cell sorting strategy was shown in the **Figure S6A**. As depicted in **Figure S6B-C,** the infiltration of CD45^{+} cells from colonic lamina propria was significantly decreased in colitic *Tmem173*$^{i\Delta mye}$ mice. Myeloid STING deletion significantly reduced the frequency of CD11b^{-}CD11c^{+} DCs and CD11b^{+}CD11c^{+} DCs in response to DSS treatment (**Figure 3A, C-D**), while CD11b^{+}CD11c^{-} myeloid cells displayed moderate increase in colitic *Tmem173*$^{i\Delta mye}$ mice without statistical significance (**Figure 3A and G**). These findings are consistent with RNA-seq analysis (**Figure 3E**). Although CD11b^{+}CD11c^{-} myeloid cells were accumulated in *Tmem173*$^{i\Delta mye}$ mice, a significant reduction of F4/80^{+}CD11b^{+}CD11c^{-} macrophages was observed (**Figure 3B and H**), suggesting abrogated maturation of macrophages. GSEA analysis and corresponding gene expressions further revealed that myeloid cell-specific STING deletion negatively regulated signaling pathways involved in macrophage migration, chemotaxis, and activation (**Figure 3F**). The potential deficiency in GM-CSF- and M-CSF-mediated macrophage differentiation (**Figure S7A**) in adult *Tmem173*$^{i\Delta mye}$ mice subjected to DSS treatment suggests a possible connection between myeloid STING and macrophage maturation. This deficiency may contribute to the disruption of immune tolerance in neonatal myeloid STING KO mice. In DSS-induced chronic colitis, similar results were found (**Figure S7B-D**). In addition to support the results of cytometry, IF analysis further demonstrated that STING activation was predominantly found in significantly infiltrated CD11b^{+}CD11c^{+} and CD11b^{+}CD11c^{-}, but not in CD11b^{-} cells in *Tmem173*$^{fl/fl}$

mice. Notably, both the infiltration of $CD11b^+$ cells and the colocalization of STING with $CD11b^+$ cells were diminished in *Tmem173*$^{i\Delta mye}$ mice (**Figure 3I-J**).

Myeloid-derived DCs have long been characterized as vital mediators of the recruitment and activation of pro-inflammatory helper T cells, including Th1, Th2, and Th17 cells [12, 13]. As expected, along with a decreased number of $CD3^+CD4^+$ T cells in colitic *Tmem173*$^{i\Delta mye}$ mice (**Figure 3K and N**), the frequencies of IFN-γ^+ Th1 and IL-17^+ Th17 cells in the lamina propria were significantly reduced (**Figure 3L and N**). However, the proportion of IL-4^+ Th2 cell remained unchanged (**Figure 3M-N**). Among these findings, the reduction of Th17 phenotype was most significant and was further supported by qPCR analysis (**Figure 3O**). A similar downregulation of *Il17a* was also seen in chronic colitis (**Figure S7E**). GSEA analysis also indicated that T cell-related pathways, including Th1 and Th17 cell differentiation, and IL-17 production were all inhibited in *Tmem173*$^{i\Delta mye}$ mice in response to DSS, when compared to *Tmem173*$^{fl/fl}$ mice (**Figure 3P**). Therefore, myeloid cell-specific STING deletion attenuated intestinal inflammation through suppressing DC and macrophage infiltration and Th1/Th17 cell activation in colon.

Figure 3

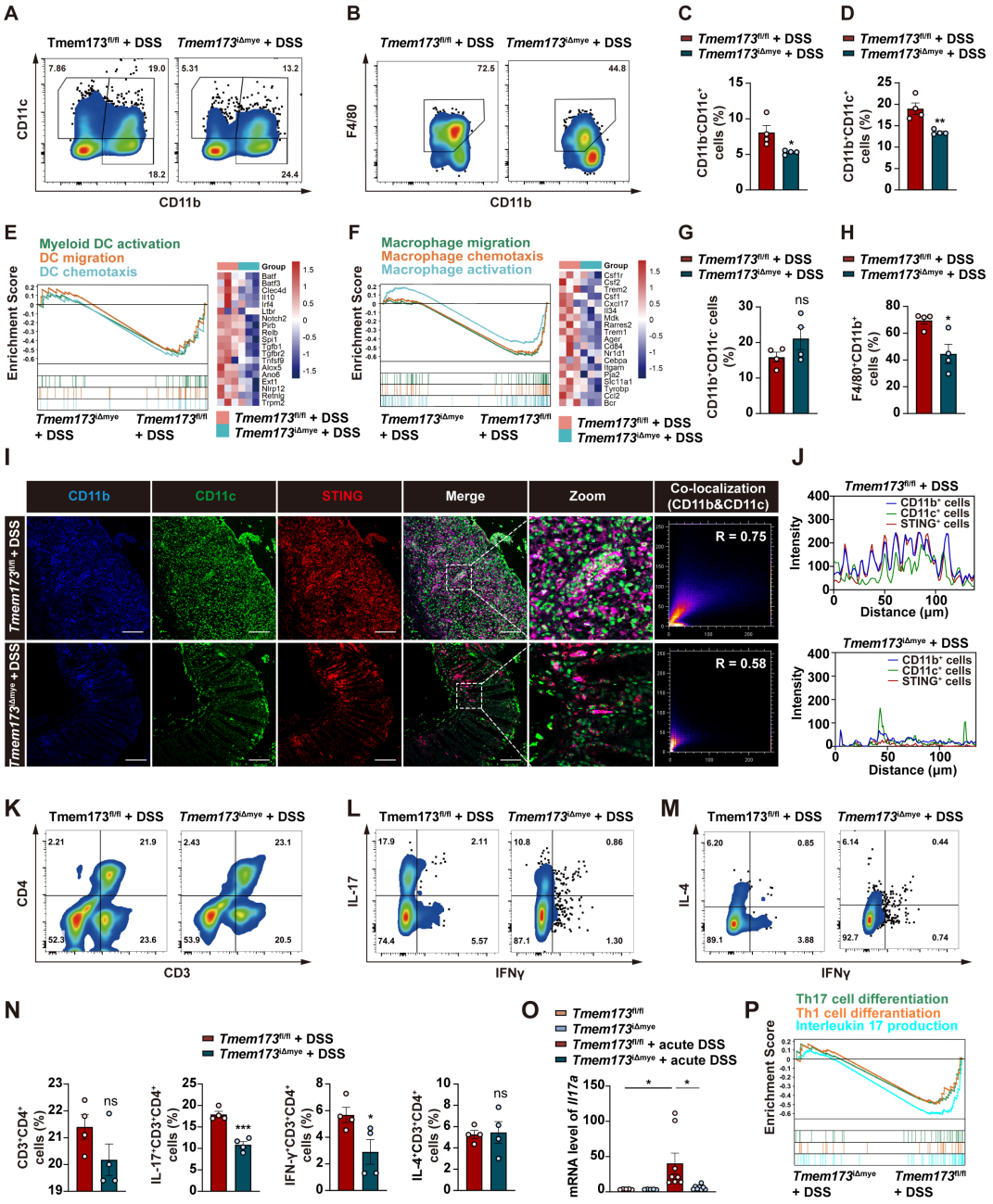

Figure 3. Effects of myeloid cell-specific STING deletion on DC and macrophage infiltration and Th1/Th17 cell activation in colitis. (A-D, G-H) Representative flow cytometry results and quantitative analysis of $CD11b^{-}CD11c^{+}$ DCs, $CD11b^{+}CD11c^{+}$ DCs, $CD11b^{+}CD11c^{-}$ monocytes and $F4/80^{+}CD11b^{+}$ macrophages in the colonic lamina propria. **(E)** GSEA analysis on pathways related to DC activation, migration, and chemotaxis in *Tmem173*$^{i\Delta mye}$ + DSS *vs* *Tmem173*$^{fl/fl}$ + DSS. The relative expression of genes in the leading-edge subset of GSEA analysis is shown alongside

as a heatmap. **(F)** GSEA analysis of pathways related to macrophage activation, migration, and chemotaxis in *Tmem173*$^{i\Delta mye}$ + DSS *vs* *Tmem173*$^{fl/fl}$ + DSS and heatmap. **(I-J)** Representative immunofluorescence co-staining of CD11b, CD11c and STING in the colon and the quantitative analysis. The co-localization of CD11b and CD11c in *Tmem173*$^{fl/fl}$ + DSS group and *Tmem173*$^{i\Delta mye}$ +DSS group were calculated with overlap coefficient R. **(K-N)** Representative flow cytometry results and quantitative analysis of $CD3^+CD4^+$ T cells, IL-17^+ $CD3^+CD4^+$ Th17 cells, IFN$\gamma^+CD3^+CD4^+$ Th1 cells, and IL-$4^+CD3^+CD4^+$ Th2 cells in the colonic lamina propria. **(O)** Relative mRNA levels of *Il17a* in the colon. **(P)** GSEA analysis on pathways related to Th1 and Th17 differentiation, and IL-17 production in *Tmem173*$^{i\Delta mye}$ + DSS *vs* *Tmem173*$^{fl/fl}$ + DSS. Scale bars, 100 μm. Values represent the mean ± S.E.M. of at least four mice in each group. Statistical significance: ns, not significant, *p < 0.05, **p < 0.01, ***p < 0.001.

T helper cell priming IL-12 family cytokines are predominantly produced by DCs in response to STING-TBK1-IRF3/NF-κB activation in colitis.

Macrophages and DCs are known to be pivotal in priming and activating Th1 and Th17 cells through IL-12 and IL-23 secretion [13-15]. As shown in **Figure 4A**, GSEA analysis indicated that in acute colitis model, IL-12/23 production and IL-12 signaling pathways were enriched in *Tmem173*$^{fl/fl}$ mice, which was verified by qPCR results (**Figure 4B**). The reduction of *Il12a*, *Il12b*, and *Il23a* expression was also observed in chronic colitis (**Figure S7F**). To further investigate whether the activation of IL-12 signaling in colitis is dependent on STING, bone marrow-derived macrophages (BMDMs) and bone marrow-derived dendritic cells (BMDCs) isolated from *Tmem173*$^{fl/fl}$ mice and *Tmem173*$^{i\Delta mye}$ mice were treated with STING agonist Vadimezan (DMXAA) and RNA-seq analysis was applied. Based on RNA-seq analysis, both BMDCs and BMDMs exhibit high expression of their respective cell-specific marker genes, confirming the purity and distinction of BMDCs and BMDMs (**Figure S8A**). As speculated, the activation of STING pathway (**Figure 4C**), inflammation-related pathways, and pathways involved in the maturation and activation of macrophages

and DCs (**Figure S8B-D**) were significantly stimulated by DMXAA in both BMDMs and BMDCs derived from *Tmem173*$^{fl/fl}$ mice. However, these effects were reversed in BMDMs and BMDCs derived from *Tmem173*$^{i\Delta mye}$ mice. Consistently, qPCR results indicated that the mRNA expression of interferon (IFN) and IFN-stimulated genes (ISGs) were significantly decreased in both STING KO BMDMs and BMDCs after DMXAA treatment (**Figure 4D**). Likewise, in RNA-seq results, IL-12 and IL-23 production-related pathways were enriched in DMXAA-treated BMDMs and BMDCs derived from *Tmem173*$^{fl/fl}$ mice, but not STING KO cells (**Figure 4E-F)**. Notably, DMXAA induced higher expression of STING downstream genes and IL-12 family cytokines in BMDCs, when compared with BMDMs. Especially, *Il12a*, *Il12b* and *Il23a* were predominantly expressed in BMDCs instead of BMDMs (**Figure 4G**). The different capacities in producing IL-12 family cytokines between BMDCs and BMDMs suggested that the activation of T helper cells in colitis were largely dependent on STING activation in myeloid-derived DCs.

Figure 4

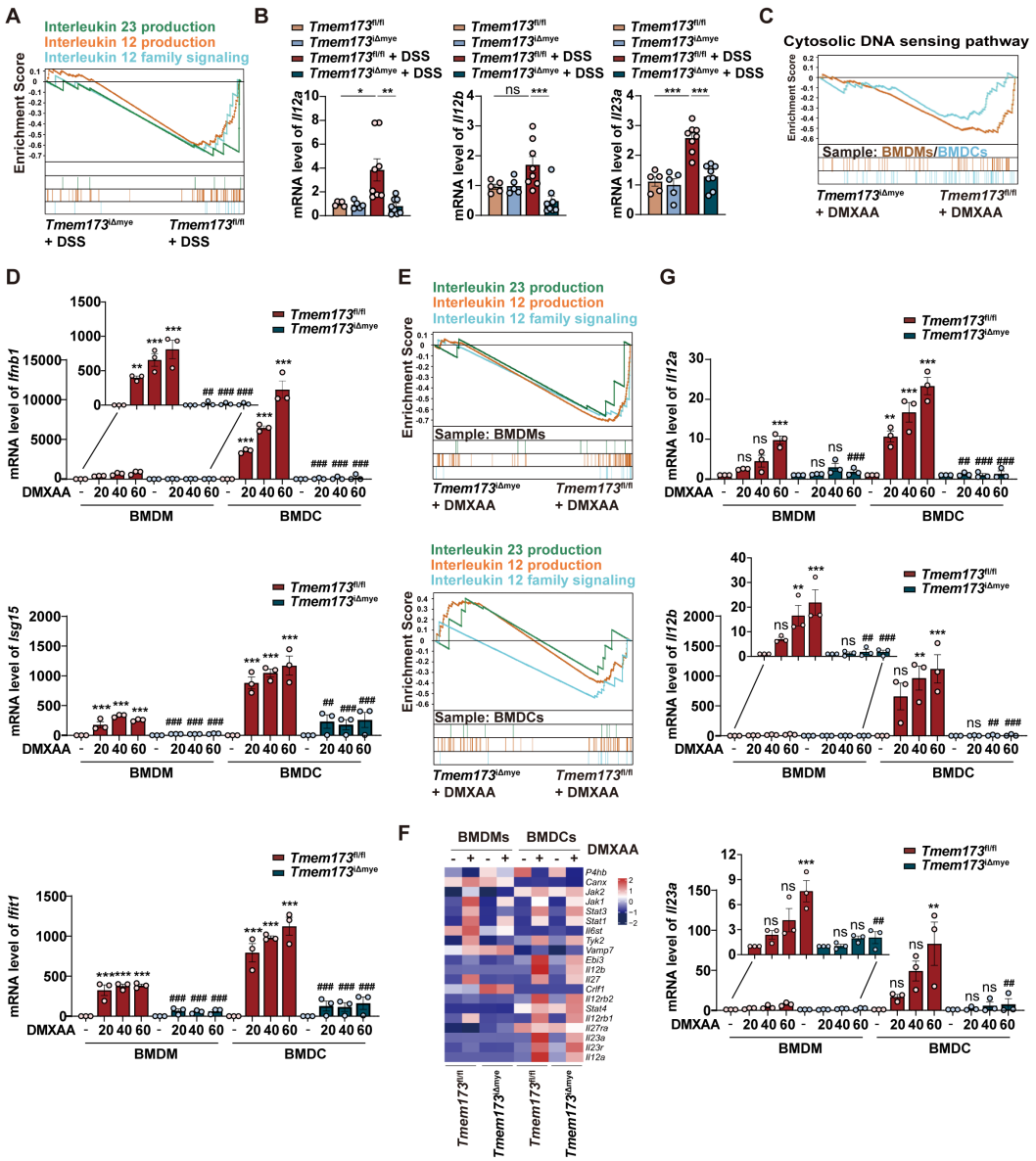

399

400 **Figure 4. Myeloid-specific knockout of STING inhibits IL12/IL23 expression *in***

401 ***vivo* and *in vitro*. (A)** GSEA analysis of IL-12 family pathways in *Tmem173*$^{i\Delta mye}$ + DSS

402 *vs Tmem173*$^{fl/fl}$ + DSS. **(B)** Relative mRNA levels of *Il12a*, *Il12b*, and *Il23a* in the colon.

403 Values represent the mean ± S.E.M. of at least five mice in each group. Statistical

404 significance: ns, no significant, *p < 0.05, **p < 0.01, ***p < 0.001. **(C-G)** WT and STING

405 KO BMDMs and BMDCs were treated with DMXAA (DX). **(C)** GSEA analysis of

406 cytosolic DNA sensing pathway in *Tmem173*$^{i\Delta mye}$ + DMXAA *vs Tmem173*$^{fl/fl}$ + DMXAA

407 in BMDMs and BMDCs. **(D)** Relative mRNA levels of *Ifnb1*, *Isg15*, and *Ifit1*. **(E)** GSEA

408 analysis of IL-12 family pathways in *Tmem173*$^{i\Delta mye}$ + DMXAA *vs Tmem173*$^{fl/fl}$ + DMXAA

in BMDMs and BMDCs, and **(F)** the relative expression of genes in the leading-edge subset. **(G)** Relative mRNA levels of *Il12a*, *Il12b*, and *Il23a* in primary BMDMs and BMDCs. Values represent the mean ± S.E.M. of at least three samples in each group. Statistical significance relative to *Tmem173*$^{fl/fl}$ group: ns, no significant, *p < 0.05, **p < 0.01, ***p < 0.001. Statistical significance relative to *Tmem173*$^{fl/fl}$ + DMXAA group: ns, not significant, $^{\#\#}$p < 0.01, $^{\#\#\#}$p < 0.001.

However, critical evidence is still lacking regarding whether IL-12 family cytokines are direct downstream targets of STING activation. As anticipated, DMXAA remarkably induced the activation of TANK-binding kinase 1 (TBK1), IRF3, and NF-κB, and the degradation of inhibitory subunit of nuclear factor kappa-B alpha (IκBα) in BMDCs (**Figure S9A**). In **Figure 5A**, TBK1 inhibitor GSK8612, IRF3 inhibitor MRT67307, and NF-κB inhibitor p-XSC were then used to elucidate the specific downstream transcription factors and signaling pathways involved in STING-mediated IL-12 expression. The effects of these inhibitors were shown in **Figure 5B-C**. GSK8612 and MRT67307 effectively inhibited the phosphorylation of TBK1 and downstream IRF3, respectively, also both slightly suppressed NF-κB activation in DMXAA-induced BMDCs. As the negative regulator of the binding of NF-κB and DNA, P-XSC had no significant influence on TBK1/IRF3 pathway and NF-κB phosphorylation. Furthermore, the expressions of type I IFN and ISGs in response to STING activation were significantly abrogated by TBK1 and IRF3 inhibitors, rather than NF-κB inhibitor, which were complied with previous reports (**Figure 5D**). However, all inhibitors attenuated the DMXAA-induced expression of IL-12 family genes, albeit with varying potencies. Interestingly, MRT67307 exhibited greater suppressive effects on *Il12a* and *Il12b* expression than p-XSC, whereas P-XSC displayed more pronounced restriction on the transcription of *Il23a* (**Figure 5E**). These effects are potentially attribute to the presence of more binding elements of IRF3 on the promoter regions of *Il12a* and *Il12b*, as well as more NF-κB binding sites on the *Il23a* promoter (**Figure 5F-G**, and **Figure S9B-D**). Functioned as a specific inhibitor of TBK1, which is the shared upstream factor

of IRF3 and NF-κB, GSK8612 consistently inhibited the expressions of all IL-12 family genes (**Figure 5E**). These findings indicated that both IRF3 and NF-κB are indispensable in the STING activation-mediated transcription of IL-12 family cytokines.

The effects of IL-12 family cytokines derived from DMXAA-treated WT and STING KO BMDCs on Th1 and Th17 differentiation of murine splenic T cells were further confirmed (**Figure 5H**). In the process of differentiating splenetic $CD3^+CD4^+$ T cells, the proportion of IL-17^+ Th17 cells and IFNγ^+ Th1 cells were found to be significantly higher when exposed to conditioned medium derived from DMXAA-treated WT BMDCs. However, these proportions decreased when exposed to conditioned medium derived from DMXAA-treated STING KO BMDCs (**Figure 5I-J**). GSEA analysis based on RNA-seq results further suggested that upregulated DEGs associated with Th1 and Th17 differentiation, IL-17 signaling, antigen-processing and presentation were all enriched in DMXAA-treated WT BMDCs, when compared with STING KO mice (**Figure S9E**). These findings demonstrate that IL-12 family cytokines are predominantly produced by DCs and favor Th1 and Th17 cell priming.

Figure 5

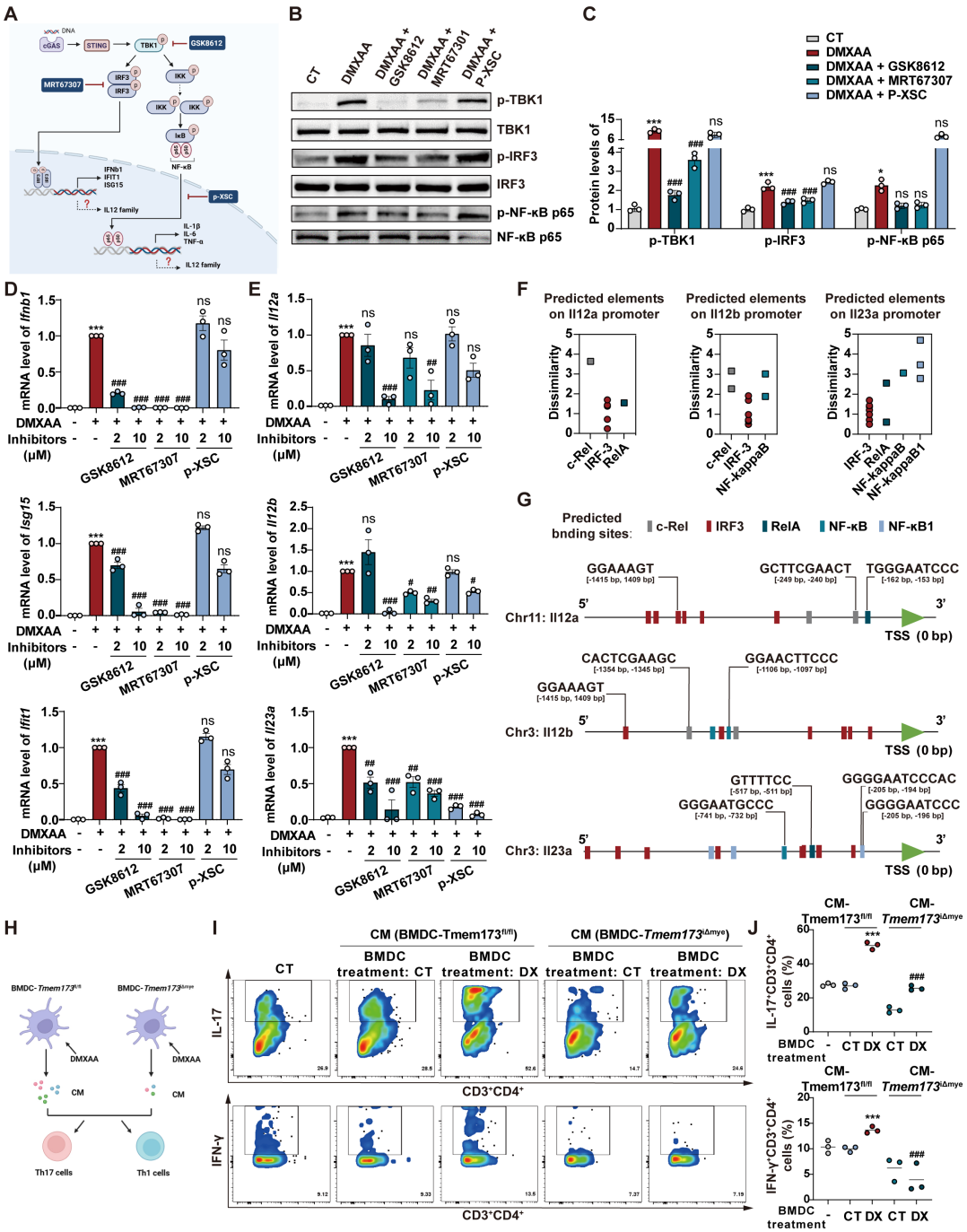

Figure 5. IRF3 and NF-κB are indispensable in the STING activation-mediated transcription of IL-12 family cytokines. (A) The Illustration of the downstream signaling cascades of STING and specific inhibitors. **(B-E)** Primary WT BMDCs were stimulated with 40 μg/mL DMXAA to activate STING pathway, with or without the treatment of GSK8612, MRT6730, and p-XSC for 8 h. **(B-C)** Representative images and quantitative analysis of immunoblotting detecting phosphorylation of TBK1, IRF3,

and NF-κB p65. **(D)** Relative mRNA levels of *Ifnb1*, *Isg15*, and *Ifit1*. **(E)** Relative mRNA levels of *Il12a*, *Il12b*, and *Il23a*. Values represent the mean ± S.E.M. of at least three samples in each group. Statistical significance relative to vehicle control: *p < 0.05, ***p < 0.001. Statistical significance relative to DMXAA group: ns, not significant, $^{\#}$p < 0.05, $^{\#\#}$p < 0.01, $^{\#\#\#}$p < 0.001. **(F)** The number and dissimilarity of predicted elements of IRF3 and NF-κB on the promoters of IL-12 family genes. **(G)** The distribution of predicted binding sites of IRF3 and NF-κB on promoters of IL-12 family cytokines. Colored boxes represent transcription factor binding sites. **(H)** Primary WT and STING KO BMDCs were stimulated with 40 μg/mL DMXAA for 8 h and the conditioned medium (CM) was collected. Differentiated splenic Th1 and Th17 cells were incubated with BMDCs-derived CM for 36 h before cells were collected for flow cytometry. **(I-J)** Representative flow cytometry results and quantitative analysis of splenic IL-17^{+} CD3^{+}CD4^{+} Th17 cells and IFNγ^{+}CD3^{+}CD4^{+} Th1 cells. Values represent the mean ± S.E.M. of at least three samples in each group. Statistical significance relative to CM(*Tmem173*$^{fl/fl}$-CT) group: ***p < 0.001. Statistical significance relative to CM(*Tmem173*$^{fl/fl}$-DX) group: $^{\#\#\#}$p < 0.001.

TFAM-associated mtDNA derived from damaged intestinal epithelial cells activates STING signaling in BMDCs to promote IL-12 signaling

In light of a recent study, we were motivated to explore whether the activation of colitis-associated myeloid STING is triggered by the intestinal microbiota [6]. We first treated mice with antibiotic cocktail (ABX) for three days before DSS administration to eliminate intestinal flora (**Figure S10A**). ABX treatment had no influence on DSS-induced elevated phosphorylation levels of STING and downstream transcription factors, including IRF3, NF-κB and IRF7 (**Figure S10B-C**). As depicted in **Figure 6A-C, and S10D**, myeloid knockout of STING still effectively attenuated DSS-induced acute colitis even though the mice were given ABX, as illustrated by elevated body weight, increased colon length, relieved disease activity, and improved colonic epithelium damage. The reduction mRNA levels of *Teme173*, pro-inflammatory

cytokines and IL-12 family genes were also found in *Tmem173*$^{i\Delta mye}$ + DSS + ABX group when compare with *Tmem173*$^{fl/fl}$ + DSS + ABX group (**Figure 6D**). Besides, in the treatment of DSS plus ABX, the activation of STING and downstream transcription factors, including IRF3, NF-κB and IRF7, were all significantly reduced in *Tmem173*$^{i\Delta mye}$ mice (**Figure S10E-F**). Since Toll-like receptors (TLRs) are the predominant sensor of microbiota-derived PAMPs and are also upstream adaptor protein of type I IFN, we treat WT and STING KO BMDMs and BMDCs with lipopolysaccharide (LPS). The deletion of STING failed to reverse the induction of type I IFN-related genes and IL-12 family genes upon LPS stimulation in BMDMs (**Figure 6E**). Likewise, the expression of *Ifnb1*, IL-12 family genes and DC marker *Cd86* still obviously increased in STING-deficient BMDCs in response to LPS (**Figure 6E**). The deletion of STING also failed to reverse the immune activation induced by other bacterial components, such as MDP (NLRs activator), peptidoglycan (TLR2 activator) and flagellin (TLR5 activator) in BMDMs and BMDCs (**Figure S10G**). The co-localization of STING, CD11b and CD11c and the numbers of $CD11b^{+}CD11c^{+}$ cells further supported above findings (**Figure S10G-H**). These data demonstrated that bacteria and bacteria-produced PAMPs are not involved in either the pathogenic roles of STING activation in colonic inflammation or the protective effects of STING deficiency against colitis.

We then hypothesized that DAMPs activated myeloid STING in response to intestinal epithelial damage. Based on the above results showing that DCs, rather than macrophages, predominantly produce IL-12 family cytokines in colitis, we conducted following experiments using BMDCs instead of BMDMs. As shown in **Figure 6F**, treatment with 100 ng/mL TNF-α resulted in significant injuries in primary colonic organoids. These injuries were characterized by PI permeabilization and epithelial destruction, which mimicked the damage observed in colitis-induced intestinal epithelial damage. The conditioned medium of damaged colonic organoids dramatically induced the expression of *Tmem173*, *Ifnb1*, *Il12a*, *Il12b,* and *Il23a* in WT BMDCs. However, these effects were almost totally blunted in STING KO BMDCs

(**Figure 6G-I**). To investigated whether DAMPs were transported *via* extracellular vesicles (EVs) system as reported previously [11], colonic organoids were pre-treated with GW4869 to inhibit the release of damage-associated EVs. Conditioned medium was also incubated with DNase and RNase to remove cell free DNA and RNA, respectively. BMDCs were co-treated with Dynasore to restrict endocytosis of either damage-associated EVs or cell free nucleotide (**Figure 6J**). Collectively, as depicted in **Figure 7F**, compared to CM (TNF-α) group, only CM (TNF-α) +DNase group and CM (TNF-α) +Dynasore group exhibited significant lower mRNA levels of *Tmem173*, *Ifnb1*, *Il12a*, *Il12b,* and *Il23a*.This suggests that the uptake of damage-associated cell free DNA through endocytosis, but not RNA or EVs, played a crucial role in activating the STING pathway in BMDCs, leading to the induction of IL-12 family gene expression (**Figure 6K**).

As anticipated, cell-free DNA fragments were released from TNF-α-damaged colonic organoids into the conditioned medium (**Figure 6L**), and were then uptake by BMDCs, as illustrated by the presence of DRAQ5-labeled damage-associated DNA fragments (**Figure 6M**). To determine the source of these DNAs, qPCR was performed to examine mitochondrial genes *mt-12S1*, *mt-Co3*, and *mt-Cytb* and nuclear gene *RN-18S*. The results showed that mtDNAs instead of nuclear DNAs were enriched in the conditioned medium derived from damaged organoids (**Figure 6N**). The removal of mtDNA by Ethidium Bromide (EtBr), a commonly used mtDNA specific eliminator, significantly blunted the expression of *Tmem173*, *Ifnb1*, *Il12a*, *Il12b,* and *Il23a* in BMDCs induced by the CM-derived damaged colonic organoid (**Figure 6O**). Notably, the protein level of mitochondrial nucleoid organizing protein TFAM was also increased in the conditioned medium (**Figure 6P**), which has been reported to enhance the detection of mtDNA by cGAS through DNA prearrangement [16]. Furthermore, through IP using a TFAM-specific antibody, we found that most of the DNA fragments in the conditioned medium were associated with TFAM and identified as mtDNA (**Figure 6Q**). The immunoprecipitated TFAM-mtDNA complex, free mtDNA isolated from the TFAM-IP precipitate, and the supernatant of TFAM-IP were prepared based on the same

volume of CM (TNF-α) used in other experiments in **Figure 6**, and were used to stimulate BMDC. As shown in **Figure 6R**, only TFAM-mtDNA complex from CM (TNF-α) could activate BMDC, while other treatments, including purified mtDNA extracted from liver (about 1.2 ng/μL final concentration as a mtDNA control) failed to trigger responses in BMDCs. These results demonstrated that TFAM-associated, but not free, mtDNA derived from damaged colonic epithelial activated STING and its downstream IL-12 signaling in BMDCs.

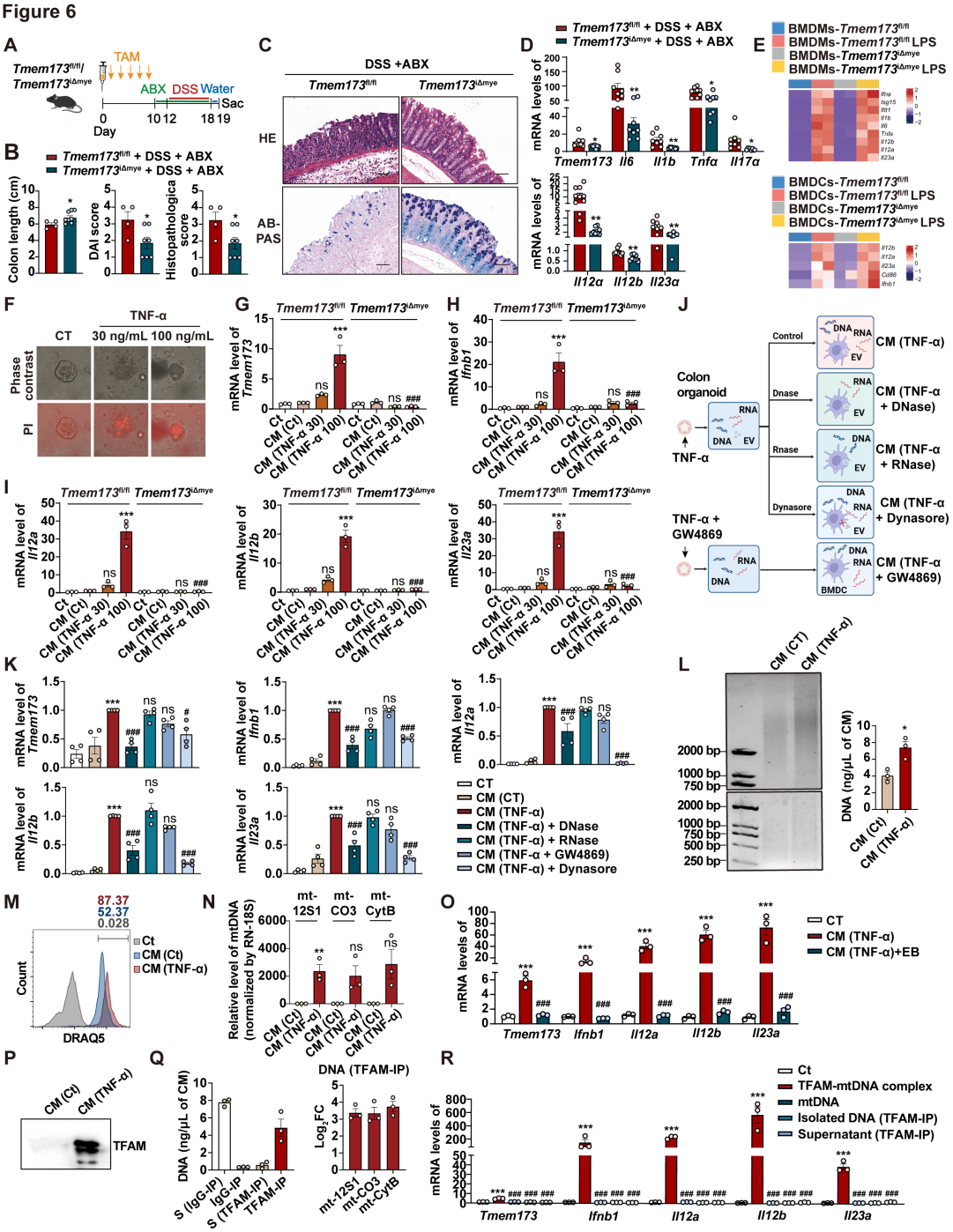

Figure 6. TFAM-associated mtDNA derived from damaged colonic organoids activates STING signaling in BMDCs to promote IL12 signaling. *Tmem173*$^{fl/fl}$ mice and *Tmem173*$^{i\Delta mye}$ mice were treated by antibiotic cocktail (ABX) and then subjected to acute DSS administration. **(A)** Animal experimental design. **(B)** Colon length, DAI score, and histopathological score. **(C)** Representative H&E and AB-PAS staining of colonic sections. Scale bars, 100 μm. **(D)** Relative mRNA levels of *Tmem173*, *Il6*, *Il1b*,

Tnfa, *Il17a*, *Il12a*, *Il12b*, and *Il23a* in the colon. Values represent the mean ± S.E.M. of at least three samples in each group. Statistical significance: *p < 0.05, **p < 0.01. **(E)** Primary WT and STING KO BMDMs and BMDCs were stimulated with LPS for 8 h. Relative mRNA levels of genes of type I IFNs and IL-12 family are shown as a heatmap. **(F-I)** The colonic organoids were treated with vehicle control or TNF-α (30 ng/mL or 100 ng/mL) and the conditioned medium (CM) was collected. **(F)** Representative images of PI staining of colonic organoids. **(G-I)** WT and STING KO BMDCs were incubated with indicated CM and the relative mRNA levels of *Tmem173*, *Ifnb1*, *Il12a*, *Il12b*, and *Il23a* gene are shown. **(J-N)** The colonic organoids were treated with vehicle control, 100 ng/mL TNF-α, or co-treated with 100 ng/mL TNF-α and 10 μM GW4869, and the CM was collected, named as CM (CT), CM (TNF-α), and CM (TNF-α+GW4869), respectively. Some CM samples were further treated by DNase (100 U/mL) and RNase (10 μg/mL), named as CM (TNF-α) + DNase and CM (TNF-α) + RNase. WT BMDCs were incubated with indicated CM with or without 80 μM Dynasore. **(K)** Relative mRNA levels of *Tmem173*, *Ifnb1*, *Il12a*, *Il12b*, and *Il23a*. **(L)** Representative image of DNA gel detecting free DNA fragments in the indicated CM. DNA concentrations are shown alongside. **(M)** The indicated CM was incubated with 5 mM DRAQ5 DNA probe. Representative flow cytometry results and quantitative analysis of DRAQ5-labeled DNA uptake in BMDCs. **(N)** The DNA levels of *mt-12S1*, *mt-CO3*, *mt-CytB*, were normalized by nuclear gene *RN-18S*. **(O)** WT BMDCs were incubated with CM (TNF-α) and EtBr-treated CM (TNF-α). Relative mRNA levels of *Tmem173*, *Ifnb1*, *Il12a*, *Il12b*, and *Il23a* are shown. **(P)** Representative image of immunoblotting detecting TFAM in the CM. **(Q)** DNA quantifications in the supernatant or precipitate from the IP experiment using IgG antibody-coated beads or anti-TFAM antibody-coated beads. The log_2FC values of *mt-12S1*, *mt-CO3*, and *mt-CytB* in immunoprecipitated TFAM-DNA complex are shown alongside. S (Supernatant). **(R)** WT BMDCs were incubated with TFAM-mtDNA complex, purified free mtDNA (mtDNA), free DNA isolated from TFAM-DNA complex (isolated DNA(TFAM-IP)), or the supernatant from TFAM-IP experiment (supernatant (TFAM-IP)). Relative mRNA levels

of *Tmem173*, *Ifnb1*, *Il12a*, *Il12b*, and *Il23a* are shown. Values represent the mean ± S.E.M. of at least three samples in each group. Statistical significance relative to Ct or CM (Ct) groups: ***p < 0.001; relative to CM (TNF-α) or TFAM-mtDNA complex groups: ###p < 0.001.

Inducing myeloid STING knockout at different time points has opposite effects on the progression of colitis-associated tumorigenesis

Patients with colitis have substantial risk of developing colitis-associated carcinoma (CAC) [17]. To further explore whether myeloid-specific STING knockout at the inflammation phase protects tumorigenesis, we established an AOM/DSS-induced CAC murine model. We intraperitoneally injected TAM into mice prior to DSS induction to ablate myeloid STING before the occurrence of inflammation (referred as *Tmem173*$^{fl/fl}$ AOM+DSS-P group and *Tmem173*$^{i\Delta mye}$ AOM+DSS-P group) (**Figure 7A**). As anticipated, following the induction of AOM/DSS, there was a notable increase in the survival rate of mice with myeloid ablation of STING compared to *Tmem173*$^{fl/fl}$ mice, while the body weight gain had no significant difference between two groups (**Figure 7B and S11A**). The deficiency of myeloid STING also resulted in significant protection against tumor development, as evidenced by reduced tumor numbers and volumes (**Figure 7C-D**). H&E staining of colon sections supported these findings (**Figure 7E**). The mRNA levels of *Tmem173*, and inflammatory genes associated with colitis progression were all significantly downregulated, while the expression of genes involved in cytotoxic lymphocyte (CTL)-mediated tumor immunity, including *Gzmb*, *Perforin*, and *Cd8* were all significantly elevated in *Tmem173*$^{i\Delta mye}$ AOM+DSS-P group, when compared with *Tmem173*$^{fl/fl}$ mice **(Figure 7F-G)**. These results demonstrate that early myeloid STING deletion can delay tumor occurrence and hinder tumor favoring cytokine-induced cell proliferation by alleviating excessive colonic inflammation. Importantly, it does not impede the process of anti-tumor immunity; instead, it enhances CTL function.

Inspired by the contrasting disease progression observed in neonatal and adult

myeloid STING KO mice, we conducted further investigations to determine if myeloid STING KO after tumor formation would yield different outcomes. We thus performed TAM administration after three circles of AOM/DSS induction (referred as *Tmem173*$^{fl/fl}$ AOM+DSS-L group and *Tmem173*$^{i\Delta mye}$ AOM+DSS-L group) (**Figure 7H**). There was no significant difference in the number and volume of tumors between these two groups before TAM induction (**Figure S11B-C**). Interestingly, the ablation of myeloid STING after tumor formation in turn lead to more severe tumor growth comparable to *Tmem173*$^{fl/fl}$ mice (**Figure 7I-L** and **Figure S11D**). Cibersort analysis baes on RNA-seq results further suggested an overall “cold” or immunosuppressive tumor environment (**Figure S12A**). The mRNA levels of *Tmem173*, tumor favoring inflammatory genes and IL-12 family genes were all remarkably increased in the tumor of *Tmem173*$^{i\Delta mye}$ mice (**Figure 7M**), in line with suppressed STING-related type I IFN pathways, and impaired antigen presentation, and macrophage and DC activation (**Figure S12B-D**). T cell chemotaxis and activation, T cell-mediated cytotoxicity and other immune responses to tumor cells were also inhibited by lateral myeloid STING KO after tumor formation (**Figure S11E-F**, and **Figure S12B-D**), which is further supported by qPCR results showing downregulated *Gzmb*, *Perforin*, and *Cd8* (**Figure 7N**)**.** As depicted in **Figure S12E**, both the number of $CD8^+$ cells and the co-localization of CD8 and Perforin were remarkably decreased in tumor of *Tmem173*$^{i\Delta mye}$ AOM+DSS-L group, suggesting a malfunction in CTL-mediated tumor immunity following myeloid STING depletion. The results indicated that deleting STING in myeloid cells before the onset of inflammation alleviated AOM/DSS-induced CAC. Conversely, eliminating STING in myeloid cells after tumor formation enhanced tumor growth by modifying the tumor microenvironment to a more immunologically inactive state.

Figure 7

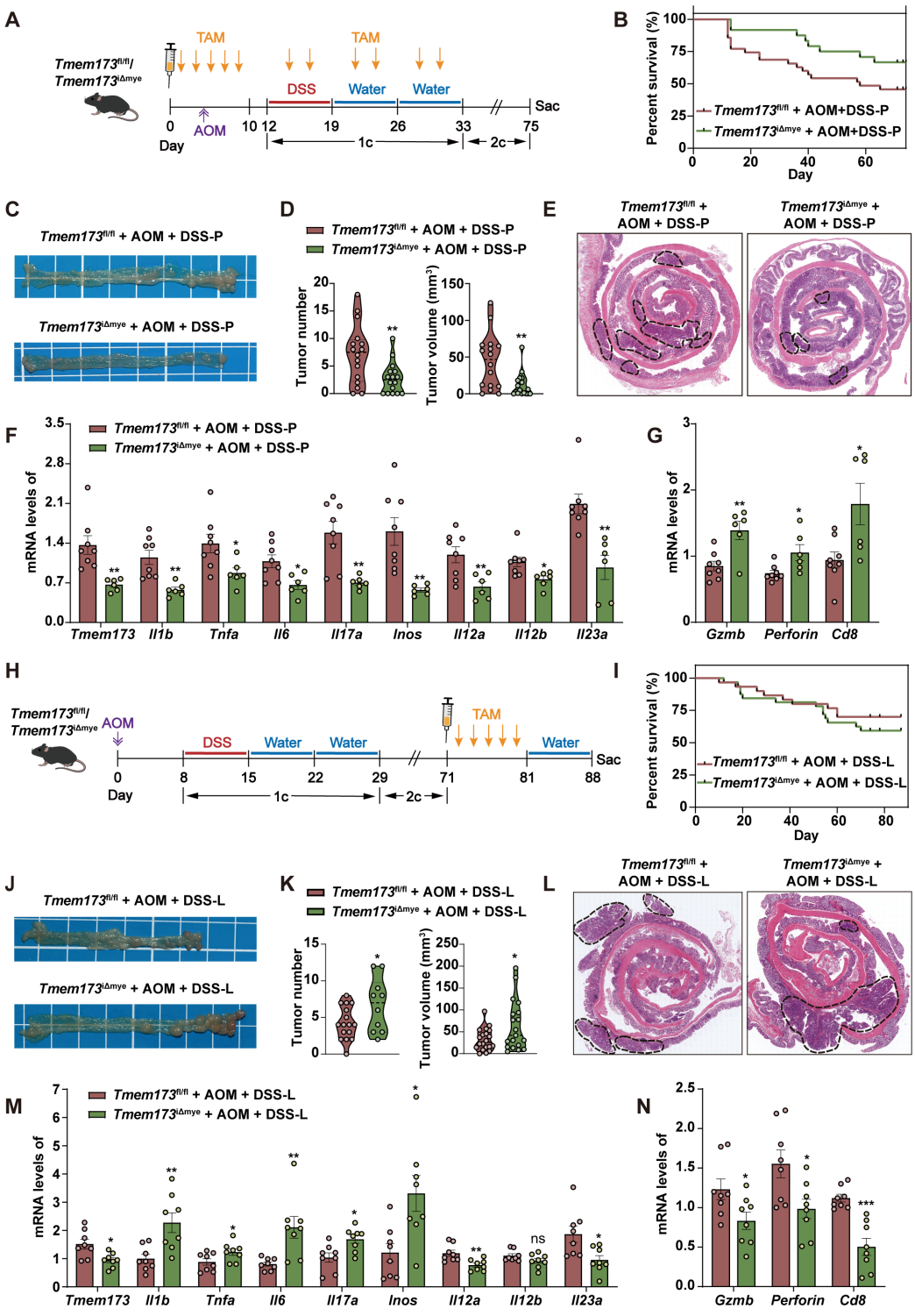

644

645 **Figure 7. Inducing myeloid STING knockout at different time points has opposite**

646 **effects on the progression of colitis-associated cancer. (A-G)** TAM administration

647 was given before the onset of inflammation in *Tmem173*$^{fl/fl}$ mice and *Tmem173*$^{i\Delta mye}$

mice in the AOM/DSS-induced CAC model. **(A)** Animal experimental design. **(B)** Survival rate. **(C)** Representative pictures of colon samples. **(D)** Tumor number and volume. **(E)** Representative H&E staining of colonic sections. **(F)** Relative mRNA levels of *Tmem173*, *Il1b*, *Tnfa*, *Il6*, *Il17a*, *Inos*, *Il12a*, *Il12b*, and *Il23a* in the normal colon tissues adjacent to tumors. **(G)** Relative mRNA levels of *Gzmb*, *Perforin*, *Cd8* in the tumors. **(H-N)** TAM administration was given after the formation of tumor in *Tmem173*$^{fl/fl}$ mice and *Tmem173*$^{i\Delta mye}$ mice in the AOM/DSS-induced CAC model. **(H)** Animal experimental flowchart. **(I)** Survival rate. **(J)** Representative colon pictures. **(K)** Tumor number and volume. **(L)** Representative H&E staining of colonic sections. **(M)** Relative mRNA levels of *Tmem173*, *Il1b*, *Tnfa*, *Il6*, *Il17a*, *Inos*, *Il12a*, *Il12b*, and *Il23a* in the normal colon tissues adjacent to tumors. **(N)** Relative mRNA levels of *Gzmb*, *Perforin*, *Cd8* in tumors. Values represent the mean ± S.E.M. of at least five mice in each group. Statistical significance: ns, no significant, *p < 0.05, **p < 0.01, ***p < 0.001.

Discussion

STING activation in myeloid cells has emerged as a critical immune factor in the pathogenesis of UC [5, 11]. In N153S mice with constitutive activation of STING, STING in CD11b$^+$ myeloid cells induced severe colonic inflammation through enhancing protein stabilization mediated by K63-linked ubiquitination [6]. Besides, Ahn and coworkers previously shown that specific knockout of STING in mononuclear phagocytes, including Lysm$^+$ cells and CD11c$^+$ cells, inhibited tumor formation in response to AOM/DSS induction [7]. In our data, myeloid deletion of STING in adult mice significantly ameliorated DSS-induced acute and chronic colitis. These results all suggested that blockade of myeloid STING may become a potential therapeutic target for the treatment of excessive inflammation in colitis and CAC. Although it was generally believed that the suppression of STING signaling effectively relieved colitis, Canesso *et al.* found that mice with congenital knockout of STING were defective in the development of mucosal barrier and intestinal immune system, which led to ultimate aggravation of colitis [10]. Moreover, it was demonstrated that ablation of

cGAS exacerbated colitis and CAC due to intestinal stem cell deficiency and impaired intestinal barrier integrity [18]. Our results also found that the deletion of myeloid SING in newborn mice exacerbated adult-onset of colonic inflammation. Despite the need for further evidence, we can infer from the accumulation of immature macrophages following myeloid STING knockout in adult mice that the congenital absence of myeloid STING may disrupt the establishment of intestinal immune homeostasis, thereby exacerbating the pathological manifestations of colitis. Notably, Zhang *et al.* recently reported that STING1 localized to the nucleus to activate transcription factor aryl hydrocarbon receptor (AHR) and competitively inhibited IRF3-meidated immune response. This nuclear STING ameliorated DSS-induced colitis by restoring gut microbial homeostasis. This finding offers another possible explanation for the protective effects of STING. However, the authors also noticed that 2'3'-cGAMP possessed higher affinity to STING when compared with the ARH ligands, and can direct AHR ligand-mediated nuclear translocation of STING to ER-ERGIC transportation, favoring canonical IRF3 activation. This suggests that nuclear STING may preferentially maintain intestinal immune tolerance in the homeostatic colon, while in the presence of DAMPs, the cGAS-STING-IRF3 pathway primarily licenses excessive inflammation [19]. The paradoxical effects of STING knockout at different stages of disease progression observed in various conditions are also evident in the colitis-associated cancer transformation process. The constraint of STING activity before cancer initiation protects against tumor development, which is consistent with a recent study [7]. However, once tumors have formed, STING deletion promotes the generation of an immunosuppressive microenvironment, thereby enhancing tumor growth. These findings emphasize the need for careful consideration of the timing of STING targeting in colitis treatment, based on the intestinal immune environment response and disease progression status, to maximize therapeutic benefits without inadvertently promoting disease progression.

Intestinal DCs are believed to function as crucial initiators and regulator of innate and adaptive immune responses in mucosal barrier. Different subsets of DCs exhibited

distinct functions on the severity of colitis in murine models [20]. Various studies have demonstrated that $CD11b^{+}CD11c^{+}$ DCs accelerated the pathogenesis of colitis by producing massive inflammatory cytokines, such as TNF-α, IL-6, IL-17, IL-12, IL-8 and IFN-γ, in DSS-induced murine model [21, 22]. Moreover, $CD11b^{+}CD11c^{+}$ DCs induced intestinal inflammation through promoting mucosal Th17 cell expansion and IL-17 responses *via* IL-23 release [14, 23, 24]. Th1 differentiation were also promoted by intestinal $CD11b^{+}CD11c^{+}$ DCs [25, 26]. In accordance with previous studies, our findings demonstrate that myeloid STING deletion effectively impairs the differentiation of Th1 and Th17 cells in colitis. This impairment in T helper cell differentiation can mostly be attributed to the reduced infiltration of $CD11b^{+}CD11c^{+}$DC cells associated with myeloid STING knockout. On the other hand, $CD11b^{-}CD11c^{+}$ DCs are helpful in maintaining intestinal mucosal tolerance and balancing the function of Treg cells and Th1 cells *via* producing retinoic acid, which is essential for the development of $Foxp3^{+}$ iTreg cells, in condition of intestinal inflammation [21, 27]. Although $CD11b^{-}CD11c^{+}$ DCs are usually not myeloid cell-derived DCs, our evidences showed that myeloid knockout of STING significantly inhibited $CD11b^{-}CD11c^{+}$ DC expansion with unknown mechanism. However, the proportion of Treg cells was not altered in colitic *Tmem173*$^{i\Delta mye}$ mice.

Clinically, heterodimer proteins IL-12 p35/p40 and IL-23 p19/p40 have been known to link innate immunity and T helper cell-mediated adaptive immunity in excessive intestinal inflammation [28-31]. Large genome-wide association studies (GWAS) also identified IL-23 receptor (IL-23R) as the susceptibility locus of UC and CD [32]. Several experimental studies further demonstrated that ubiquitous transgenic expression of IL-23 p19 contributed to severe colitis [33] and knockdown of IL-12/IL23 p40 ameliorated intestinal inflammation in various experimental colitis model [34]. Since patients with IBD lost response to TNF inhibitors after long-term treatment in clinical practice, the exploration of biological agents targeting IL-12 and IL-23 is emerging, such as ustekinumab, briakinumab, guselkumab, brazikumab and mirikizumab. Our results indicated that the absence of myeloid STING significantly

decreased the levels of *Il12b*, *Il12a*, and *Il23a* in colitis and the deletion of STING in DMXAA-treated BMDMs/BMDCs noticeably suppressed pathways related to the IL-12 family and IL-12/IL-23 production. We further confirmed that the production of *Il12b* and *Il23a* in response to STING activation is primarily observed in BMDCs rather than BMDMs, which is in line with previous studies [35]. Intriguingly, tissue-infiltrating neutrophils have also been identified as a potential source of IL-23 production [36], and the proportion of neutrophils was found potentially decreased upon myeloid STING KO in our study. Therefore, neutrophil function and neutrophil-mediated IL-23 release in the development is also worth further discovery.

Our findings further addressed more critical questions: what stimulus activate STING in BMDCs, and how does STING activation directly regulate the transcription of the IL-12 family? Emerging evidences demonstrated that the damage to mucosal barrier integrity could trigger subsequent inflammatory cascade responses, including cGAS-STING pathway sensing damage-related endogenous or bacterial dsDNA [37, 38]. Contrary to the previous belief that damage-associated EV or gut microbiota-secreted c-di-GMP mediate STING activation in the colon, our research suggests that following intestinal epithelial cell damage, cell membrane rupture leads to the release of TFAM-associated mtDNA into the tissue space, ultimately mediates STING activation as DAMPS. Moreover, the association of mtDNA with certain protein scaffold and endocytosis-mediated uptake are essential for the sensing of these protein-mtDNA complex by cGAS pathway in DC cells and downstream upregulation of IL-12 family cytokines. The activation of STING can further induce the expression of type I IFNs and ISGs through the classical IRF3 pathway or mediate the phosphorylation of IKKε, leading to non-canonical crosstalk with the NF-κB pathway. However, it remains unclear whether STING activation can directly regulate the transcription of IL-12 family cytokines, and whether this regulatory mechanism depends on selective IRF3 activation or IKKε phosphorylation. Although previous studies have reported that in many inflammatory or autoimmune diseases, the activation of NF-κB is the main regulatory mechanism for the transcription of IL-12 and IL-23 [39-41]. However, there

is a lack of experimental evidence regarding whether IRF3 can regulate the expression of IL-12 family genes. Based on our research, although it is difficult to draw conclusive and exclusive conclusions, both IRF3 and NF-κB are crucial and indispensable for the induction of IL-12 family cytokines. Our study only utilized inhibitors, which posed limitations in terms of inhibitor specificity, thus further research using genetic knockout approaches is warranted. Nonetheless, it is encouraging that we have indeed identified multiple potential binding sites for IRF3 in the promoter regions of IL-12 family genes, even more than NF-κB binding sites. This finding suggests that the activation of the downstream IRF3 pathway of STING, not only through type I IFNs, but also directly through the transcription of inflammatory cytokines, can directly participate in the regulation of adaptive immunity, opening up new avenues of research.

In summary, our study demonstrated that myeloid-specific deletion of STING in adult mice significantly ameliorated acute and chronic experimental colitis and provided protection against tumorigenesis. We also identified that damaged colonic epithelial cells released a protein-mtDNA complex, activating the STING-IRF3/NF-κB pathway in DCs. Myeloid STING knockout suppressed the expression of IL-12 family cytokines in DCs, leading to an improvement in colonic immune homeostasis by regulating Th1 and Th17 cell differentiation.

Conclusion

Our findings comprehensively analyzed STING activation in colitis, shedding light on its origin, target cells, downstream signaling pathways, and effects on adaptive immunity. This study offers compelling evidence to support the targeted inhibition of STING activity for the treatment of colitis and related inflammatory cancer transformation, presenting new avenues for innovative therapeutic strategies.

Abbreviations

ABX: antibiotic cocktail; AHR: aryl hydrocarbon receptor; BMDCs: bone marrow-derived dendritic cells; BMDMs: bone marrow-derived macrophages; CAC: colitis-

associated carcinoma; cGAMP: 2′3′ cyclic GMP-AMP; cGAS: cyclic GMP-AMP synthase; CRC: colorectal cancer; CTL: cytotoxic lymphocyte; DAMPs: damage-associated molecular patterns; DMXAA: Vadimezan; DSS: dextran sodium sulfate; ER: endoplasmic reticulum; EtBr: Ethidium Bromide; EVs: extracellular vesicles; FBS: fetal bovine serum; GWAS: genome-wide association studies; IFN: interferon; IL-23R: IL-23 receptor; IP: immunoprecipitation; IRF3: interferon regulatory factor 3; ISGs: interferon-stimulated genes; IκBα: inhibitory subunit of nuclear factor kappa-B alpha; KO: knockout; LPS: lipopolysaccharide; MyD88: myeloid-differentiation primary response protein; NF-κB: nuclear factor kappa-B; PCA: principal component analysis; PRRs: pattern recognition receptors; STING: stimulator of interferon genes; TAM: tamoxifen; TBK1: TANK-binding kinase; TLRs: Toll-like receptors; TNF: tumor necrosis factor; 5-ASA: 5-aminosalycilates.

Acknowledgements

This work was supported by the Excellent Young Scientists Fund, National Natural Science Foundation of China (Grant No. 82322075 to RL).

Authors' contributions

YC investigation, data curation, formal analysis, methodology, visualization, writing-Original Draft; SL investigation, data curation, formal analysis, methodology, visualization, writing-Original Draft; YY methodology, visualization; SD investigation, methodology, data curation; GF investigation; JB investigation, visualization; QZ visualization; YG methodology; XL resources, project administration; RL conceptualization, funding acquisition, project administration, resources, supervision, writing-review and editing.

Ethics committee approval

All animal studies were conducted in accordance with the guidelines approved by the Institutional Animal Care and Use Committee at Beijing University of Chinese Medicine guidelines (BUCM-4-2022012001-1096).

Data availability statement

The raw RNA-seq data in our analyses have been uploaded to Gene Expression Omnibus database (https://www.ncbi.nlm.nih.gov/geo) under accession number: GSE252100, GSE252101, GSE252099. Additional data, analytic methods, and study materials will be made available to researchers upon request.

Competing interests

The authors have declared that no competing interest exists.

References

1. Ordás I, Eckmann L, Talamini M, Baumgart DC, Sandborn WJ. Ulcerative colitis. Lancet. 2012; 380: 1606-19.
2. Fukata M, Arditi M. The role of pattern recognition receptors in intestinal inflammation. Mucosal Immunol. 2013; 6: 451-63.
3. Decout A, Katz JD, Venkatraman S, Ablasser A. The cGAS-STING pathway as a therapeutic target in inflammatory diseases. Nat Rev Immunol. 2021; 21: 548-69.
4. Li S, Fan G, Li X, Cai Y, Liu R. Modulation of type I interferon signaling by natural products in the treatment of immune-related diseases. Chin J Nat Med. 2023; 21: 3-18.
5. Flood P, Fanning A, Woznicki JA, Crowley T, Christopher A, Vaccaro A, et al. DNA sensor-associated type I interferon signaling is increased in ulcerative colitis and induces JAK-dependent inflammatory cell death in colonic organoids. Am J Physiol Gastrointest Liver Physiol. 2022; 323: G439-g60.
6. Shmuel-Galia L, Humphries F, Lei X, Ceglia S, Wilson R, Jiang Z, et al. Dysbiosis exacerbates colitis by promoting ubiquitination and accumulation of the innate immune adaptor STING in myeloid cells. Immunity. 2021; 54: 1137-53.e8.
7. Ahn J, Son S, Oliveira SC, Barber GN. STING-Dependent Signaling Underlies IL-10 Controlled Inflammatory Colitis. Cell Rep. 2017; 21: 3873-84.
8. Martin GR, Blomquist CM, Henare KL, Jirik FR. Stimulator of interferon genes (STING) activation exacerbates experimental colitis in mice. Sci Rep. 2019; 9: 14281.
9. Yang W, Yu T, Zhou G, Yao S, Wakamiya M, Hu H, et al. Intrinsic STING Switches off Pathogenetic Programs of Th1 Cells to Inhibit Colitis. Cell Mol Gastroenterol Hepatol. 2023; 15: 1161-79.
10. Canesso MCC, Lemos L, Neves TC, Marim FM, Castro TBR, Veloso É S, et al. The cytosolic sensor STING is required for intestinal homeostasis and control of inflammation. Mucosal Immunol. 2018; 11: 820-34.
11. Zhao F, Zheng T, Gong W, Wu J, Xie H, Li W, et al. Extracellular vesicles package dsDNA to aggravate Crohn's disease by activating the STING pathway. Cell Death Dis. 2021; 12: 815.
12. Geremia A, Biancheri P, Allan P, Corazza GR, Di Sabatino A. Innate and adaptive immunity in inflammatory bowel disease. Autoimmun Rev. 2014; 13: 3-10.
13. Zhou J, Lai W, Yang W, Pan J, Shen H, Cai Y, et al. BLT1 in dendritic cells promotes Th1/Th17 differentiation and its deficiency ameliorates TNBS-induced colitis. Cell Mol Immunol. 2018; 15: 1047-56.
14. Jin J, Jung IH, Moon SH, Jeon S, Jeong SJ, Sonn SK, et al. CD137 Signaling Regulates Acute Colitis via RALDH2-Expressing CD11b(-)CD103(+) DCs. Cell Rep. 2020; 30: 4124-36.e5.
15. Hue S, Ahern P, Buonocore S, Kullberg MC, Cua DJ, McKenzie BS, et al. Interleukin-23 drives innate and T cell-mediated intestinal inflammation. J Exp Med. 2006; 203: 2473-83.
16. Andreeva L, Hiller B, Kostrewa D, Lässig C, de Oliveira Mann CC, Jan Drexler D, et al. cGAS senses long and HMGB/TFAM-bound U-turn DNA by forming protein-DNA ladders. Nature. 2017; 549: 394-8.
17. Terzić J, Grivennikov S, Karin E, Karin M. Inflammation and colon cancer. Gastroenterology. 2010; 138: 2101-14.e5.
18. Hu S, Fang Y, Chen X, Cheng T, Zhao M, Du M, et al. cGAS restricts colon cancer development by protecting intestinal barrier integrity. Proc Natl Acad Sci U S A. 2021; 118.

19. Zhang R, Yu C, Zeh HJ, Wang H, Kroemer G, Klionsky DJ, et al. Nuclear localization of STING1 competes with canonical signaling to activate AHR for commensal and intestinal homeostasis. Immunity. 2023.
20. Bilsborough J, Viney JL. Gastrointestinal dendritic cells play a role in immunity, tolerance, and disease. Gastroenterology. 2004; 127: 300-9.
21. Hwang J, Jin J, Jeon S, Moon SH, Park MY, Yum DY, et al. SOD1 suppresses pro-inflammatory immune responses by protecting against oxidative stress in colitis. Redox Biol. 2020; 37: 101760.
22. Li J, Shi W, Sun H, Ji Y, Chen Y, Guo X, et al. Activation of DR3 signaling causes loss of ILC3s and exacerbates intestinal inflammation. Nat Commun. 2019; 10: 3371.
23. Figliuolo da Paz V, Jamwal DR, Gurney M, Midura-Kiela M, Harrison CA, Cox C, et al. Rapid Downregulation of DAB2 by Toll-Like Receptor Activation Contributes to a Pro-Inflammatory Switch in Activated Dendritic Cells. Front Immunol. 2019; 10: 304.
24. Schlitzer A, McGovern N, Teo P, Zelante T, Atarashi K, Low D, et al. IRF4 transcription factor-dependent CD11b+ dendritic cells in human and mouse control mucosal IL-17 cytokine responses. Immunity. 2013; 38: 970-83.
25. Cerovic V, Houston SA, Scott CL, Aumeunier A, Yrlid U, Mowat AM, et al. Intestinal CD103(-) dendritic cells migrate in lymph and prime effector T cells. Mucosal Immunol. 2013; 6: 104-13.
26. Cerovic V, Bain CC, Mowat AM, Milling SW. Intestinal macrophages and dendritic cells: what's the difference? Trends Immunol. 2014; 35: 270-7.
27. Muzaki AR, Tetlak P, Sheng J, Loh SC, Setiagani YA, Poidinger M, et al. Intestinal CD103(+)CD11b(-) dendritic cells restrain colitis via IFN-γ-induced anti-inflammatory response in epithelial cells. Mucosal Immunol. 2016; 9: 336-51.
28. Monteleone G, Biancone L, Marasco R, Morrone G, Marasco O, Luzza F, et al. Interleukin 12 is expressed and actively released by Crohn's disease intestinal lamina propria mononuclear cells. Gastroenterology. 1997; 112: 1169-78.
29. Brand S. Crohn's disease: Th1, Th17 or both? The change of a paradigm: new immunological and genetic insights implicate Th17 cells in the pathogenesis of Crohn's disease. Gut. 2009; 58: 1152-67.
30. Mannon PJ, Fuss IJ, Mayer L, Elson CO, Sandborn WJ, Present D, et al. Anti-interleukin-12 antibody for active Crohn's disease. N Engl J Med. 2004; 351: 2069-79.
31. Neurath MF. IL-12 family members in experimental colitis. Mucosal Immunol. 2008; 1 Suppl 1: S28-30.
32. Duerr RH, Taylor KD, Brant SR, Rioux JD, Silverberg MS, Daly MJ, et al. A genome-wide association study identifies IL23R as an inflammatory bowel disease gene. Science. 2006; 314: 1461-3.
33. Wiekowski MT, Leach MW, Evans EW, Sullivan L, Chen SC, Vassileva G, et al. Ubiquitous transgenic expression of the IL-23 subunit p19 induces multiorgan inflammation, runting, infertility, and premature death. J Immunol. 2001; 166: 7563-70.
34. Verstockt B, Salas A, Sands BE, Abraham C, Leibovitzh H, Neurath MF, et al. IL-12 and IL-23 pathway inhibition in inflammatory bowel disease. Nat Rev Gastroenterol Hepatol. 2023; 20: 433-46.
35. Becker C, Wirtz S, Blessing M, Pirhonen J, Strand D, Bechthold O, et al. Constitutive p40 promoter activation and IL-23 production in the terminal ileum mediated by dendritic cells. J Clin Invest. 2003; 112: 693-706.

921 36. Kvedaraite E, Lourda M, Ideström M, Chen P, Olsson-Åkefeldt S, Forkel M, et al. Tissue-
922 infiltrating neutrophils represent the main source of IL-23 in the colon of patients with IBD. Gut.
923 2016; 65: 1632-41.
924 37. Vereecke L, Beyaert R, van Loo G. Enterocyte death and intestinal barrier maintenance in
925 homeostasis and disease. Trends Mol Med. 2011; 17: 584-93.
926 38. Torres J, Mehandru S, Colombel JF, Peyrin-Biroulet L. Crohn's disease. Lancet. 2017; 389:
927 1741-55.
928 39. Poladian N, Orujyan D, Narinyan W, Oganyan AK, Navasardyan I, Velpuri P, et al. Role of NF-
929 κB during Mycobacterium tuberculosis Infection. Int J Mol Sci. 2023; 24.
930 40. Wang N, Liang H, Zen K. Molecular mechanisms that influence the macrophage m1-m2
931 polarization balance. Front Immunol. 2014; 5: 614.
932 41. Gu L, Ning H, Qian X, Huang Q, Hou R, Almourani R, et al. Suppression of IL-12 production
933 by tristetraprolin through blocking NF-kcyB nuclear translocation. J Immunol. 2013; 191: 3922-30.
934

Supplementary materials

Materials and methods

AOM/DSS-induced colitis-associated carcinoma (CAC) model

The ablation of myeloid STING before the occurrence of inflammation was referred as *Tmem173*$^{fl/fl}$ AOM+DSS-P group and *Tmem173*$^{i\Delta mye}$ AOM+DSS-P group. 5 to 6-week-old *Tmem173*$^{fl/fl}$ mice and *Tmem173*$^{i\Delta mye}$ mice were injected intraperitoneally with 10 mg/kg Azoxymethane (AOM; Sigma, Missouri, USA) in the middle of five-time continuous tamoxifen induction. One week later, the mice were administered with 2.5% DSS for 7 days every 3 weeks. This process was repeated 3 times.

The ablation of myeloid STING after the formation of tumor was referred as *Tmem173*$^{fl/fl}$ AOM+DSS-L group and *Tmem173*$^{i\Delta mye}$ AOM+DSS-L group. Tamoxifen induction was performed after three-time DSS cycles followed by one week and the mice were sacrificed. The body weight of mice was monitored every day. Tumor tissue and colon tissue adjacent tumor were harvested at the end of the experiment.

Antibiotic cocktail experiment

C57BL/6N mice, *Tmem173*$^{fl/fl}$ mice and *Tmem173*$^{i\Delta mye}$ mice at the age of 6 to 8-week-old were orally treated with 300 μL antibiotic cocktail (ABX), supplemented with 8 g/L Ampicillin Na, 4 g/L Vancomycin HCL, 8 g/L Neomycin sulfate, and 8 g/L Metronidazole three days before DSS induction and till the end of experiment.

The assessment of disease activity index (DAI) score

DAI score was calculated as the mean value of three parameters, including weight loss, stool consistency, and gross bleeding. The weight loss was graded as follows: 0, none; 1, 1%-5%; 2, 5%-10%; 3, 10%-20%; 4, >20%. The stool consistency was graded as follows: 0, normal; 2, loose; 4, diarrhea. The gross bleeding was graded as follows: 0, absence; 2, blood tinged; 4, presence.

Histological analysis and Alcian blue-Periodic acid Schiff (AB-PAS) staining

Proximal colonic specimens were fixed in 10% neutral buffered formalin for 24 h before undergoing dehydration and embedding in paraffin. Hematoxylin and eosin

(H&E) staining was performed on 5 μm sections. The histopathological score was evaluated according to the following criteria: epithelial structure loss; crypt abscess formation; inflammatory leukocyte infiltration; goblet cell number loss; muscle layer hyperplasia. Each parameter was scored from 0 to 3. The colonic sections were also stained with AB-PAS under the guidance of corresponding staining kit (Solarbio, Beijing, China) to visualize the changes in goblet cells and mucin expression.

Quantitative real-time PCR (qPCR) analysis

Total RNA of colonic tissues was extracted and purified by lithium chloride (Sigma, Missouri, USA) to counteract the suppression of DSS on qPCR process. 1 μg of RNA was reverse transcribed using HiScript III RT SuperMix for qPCR (Vazyme, Nanjing, China). 10 ng of cDNA was then subjected to perform qPCR analysis using AceQTM Universal SYBR Qpcr Master Mix (Vazyme, Nanjing, China). Gene expressions were normalized by HPRT1. Primer sequences of qPCR will be provided as requested.

Western blot analysis

Total colonic tissues were lysed with RIPA. The concentrations of protein were measured by BCA protein assay kit (Biorigin, Beijing, China). Equal amount of protein was subjected to SDS-polyacrylamide gel and transferred to polyvinylidene fluoride (PVDF) membranes. The membranes were blocked with 5% non-fat milk powder and incubated overnight at 4 °C with various primary antibodies against p-STING (Ser366) (Cell signaling Technology, Massachusetts, USA, 50907), STING (Proteintech, Chicago, USA, 19851-1-AP), p-TBK1/NAK (Ser172) (Cell signaling Technology, Massachusetts, USA, 5483S), TBK1/NAK (Cell signaling Technology, Massachusetts, USA, 38066S), p-IRF-3 (Ser396) (Cell signaling Technology, Massachusetts, USA, 29047S), IRF-3 (Cell signaling Technology, Massachusetts, USA, 4302S), p-NF-κB P65 (ser468) (Proteintech, Chicago, USA, 82335-1-RR), NF-KB p65 (Proteintech, Chicago, USA, 10745-1-AP), IκBα (Proteintech, Chicago, USA, 10268-1-AP), IRF7 (Proteintech, Chicago, USA, 22392-1-AP). The membranes were then incubated with anti-rabbit IgG or anti-mouse IgG antibody (Proteintech, Chicago, USA). Protein levels were normalized by Beta Actin antibody (Proteintech, Chicago, USA, 66009-1-lg) as a

control.

Immunofluorescence analysis

Colonic tissue sections were dewaxed and rehydrated through gradient alcohols. The hidden antigens were exposed by 1 mM citrate antigen retrieval solution (Beyotime, Shanghai, China) and then were blocked with 10% normal goat serum (Solarbio, Beijing, China). The sections were incubated with primary antibodies against STING (Proteintech, Chicago, USA, 19851-1-AP) and CD11B/Integrin Alpha (Proteintech, Chicago, USA, 66519-1-Ig) overnight at 4 °C. Signals were detected by goat anti-mouse IgG (H+L) Alexa Fluor Plus 488 (Thermo Fisher Scientific, Massachusetts, USA, A32723) and anti-rabbit IgG (H+L) Alexa Fluor 594 conjugate (Cell Signaling Technology, Massachusetts, USA, 8889S), and then counterstained with DAPI (Abcam, London, US). The sections were incubated with primary antibodies against STING, CD11B/Integrin Alpha and CD11/Integrin alpha (Proteintech, Chicago, USA, 60258-1-Ig) and multiple immunofluorescences were performed according to the manufacture's instruction of four-color fluorescence kit (Recordbio, Shanghai, Beijing). The co-localization of indicated targets were measured with the overlapping coefficient R calculated by plugin Colocalization Finder in software ImageJ.

RNA-sequencing and data analysis

The RNA-Sequencing was performed by Novogene Co., Ltd. (Beijing, China) as previously described [1]. Differentially expressed genes were analyzed by DESeq2 R package (version 1.20.0) with the threshold of |log2FoldChange| >= 1 and p-value <= 0.05. Gene Ontology (GO) and Kyoto Encyclopedia of Genes and Genomes (KEGG) enrichment analysis were performed using the ClusterProfiler R package (version 3.8.1) through R programming language (version 4.3.1). Gene Set Enrichment Analysis (GSEA) was determined by local version of the GSEA analysis tool http://www.broadinstitute.org/gsea/index.jsp. The immune cell infiltration analysis was performed according to RNA-seq data by local version of CIBERSORT tool and single sample gene set enrichment analysis (ssGSEA) tool. The RNA-seq results of the acute colitis experiment (Accession number GSE252100), the RNA-seq results of the BMDM

and BMDC experiments (Accession number GSE252101), and the RNA-seq results of the AOM/DSS experiment (Accession number GSE252099) are available in Gene Expression Omnibus. Each group contains three randomly selected samples for acute colitis experiment, BMDM and BMDC experiments, and AOM/DSS experiment.

Flow cytometry analysis

To analyze the innate immune responses, LP cells were stained with anti-CD45 FITC (Biolegend, California, USA, 103108), anti-CD11B Alexa Flour 700 (Biolegend, California, USA, 101222), anti-CD11C APC (Biolegend, California, USA, 117310), anti-F4/80 PE (Biolegend, California, USA, 123110) and Zombie NIR (Biolegend, California, USA, 423105). To analyze the adaptive immune responses, isolated LP cells were incubated with leukocyte activation cocktail (BD, New Jersey, USA, 550583) overnight for 10h. Then the activated LP cells were stained with anti-CD45 PerCP (Biolegend, California, USA, 103129), anti-CD3 AF488 (Biolegend, California, USA, 100210), anti-CD4 BV421 (RM4-5 clone) (Biolegend, California, USA, 100563), anti-IFN-γ AF647 (BD, New Jersey, USA, 557735), anti-IL-17 BV605 (BD, New Jersey, USA, 564169), anti-IL-4 PE (Biolegend, California, USA, 504103) and Zombie NIR (Biolegend, California, USA, 423105). The data analysis of flow cytometry was done with the FlowJo software.

The isolation and differentiation of bone marrow-derived macrophages (BMDMs) and bone marrow-derived dendritic cells (BMDCs)

Bone marrow-derived cells were isolated from the femur and tibia bones of *Tmem173*$^{fl/fl}$ mice and *Tmem173*$^{i\Delta mye}$ mice. BMDMs were differentiated from bone marrow-derived cells by culturing with fresh DPMI1640 medium containing 10% FBS, 1% penicillin-streptomycin solution (P/S), and 10% cultured supernatant of L929 cells for 7 days. Medium was replaced every two days. BMDCs were obtained from bone marrow-derived cells by culturing with fresh DPMI1640 medium containing 10% FBS, 1% P/S, 20 ng/mL GM-CSF and 10 ng/mL IL-4 for 7 days. Medium was replaced every two days. For *in vitro* studies, cells were placed into the 6-well plate and administrated with DMXAA (20, 40, 60 μg/mL), LPS (50 ng/mL), MDP (200 ng/mL), Flagellin (200

ng/mL), peptidoglycan (10 μg/mL), CM(CT), CM(TNF-α), TFAM-mtDNA complex, purified mtDNA (mtDNA isolated from fresh mouse liver using the tissue mitochondria isolation kit (Beyotime, China)), isolated DNA (TFAM-IP), and supernatant (TFAM-IP) as indicated. To be note, all doses of the other treatments in **Figure 6** are equivalent to the dose of CM (TNF-α). To be more specific, the immunoprecipitated TFAM-mtDNA complex, free mtDNA isolated from the TFAM-IP precipitate, and the supernatant of TFAM-IP were all prepared based on the same volume (500 μL) of CM (TNF-α)

The isolation and differentiation of splenetic Th1 and Th17 cells

Splenetic $CD4^+$ T cells were isolated under the guidance of EasySep™ Mouse $CD4^+CD62L^+$ T Cell Isolation Kit (Stemcell, Vancouver, Canada). Isolated $CD4^+$ T cells were incubated with anti-CD3 and anti-CD28 overnight to induce activation. To be differentiated into Th1 cells, the activated $CD4^+$ T cells were induced by 4 ng/mL IL-2, 10 ng/mL IL-12 and 10 μg/mL anti-IL-4 for three days. To be differentiated into Th17 cells, the activated $CD4^+$ T cells were induced by 50 ng/mL IL-6, 5 ng/mL TGF-β, 10 μg/mL anti-IFNγ, 10 μg/mL anti-IL-4, and 4 ng/mL IL-2 for three days. The differentiated Th1 and Th17 cells were incubated with supernatant of CT or DMXAA-treated BMDCs from *Tmem173*$^{fl/fl}$ mice or *Tmem173*$^{i\Delta mye}$ mice for 36 h. and then perform flow cytometry.

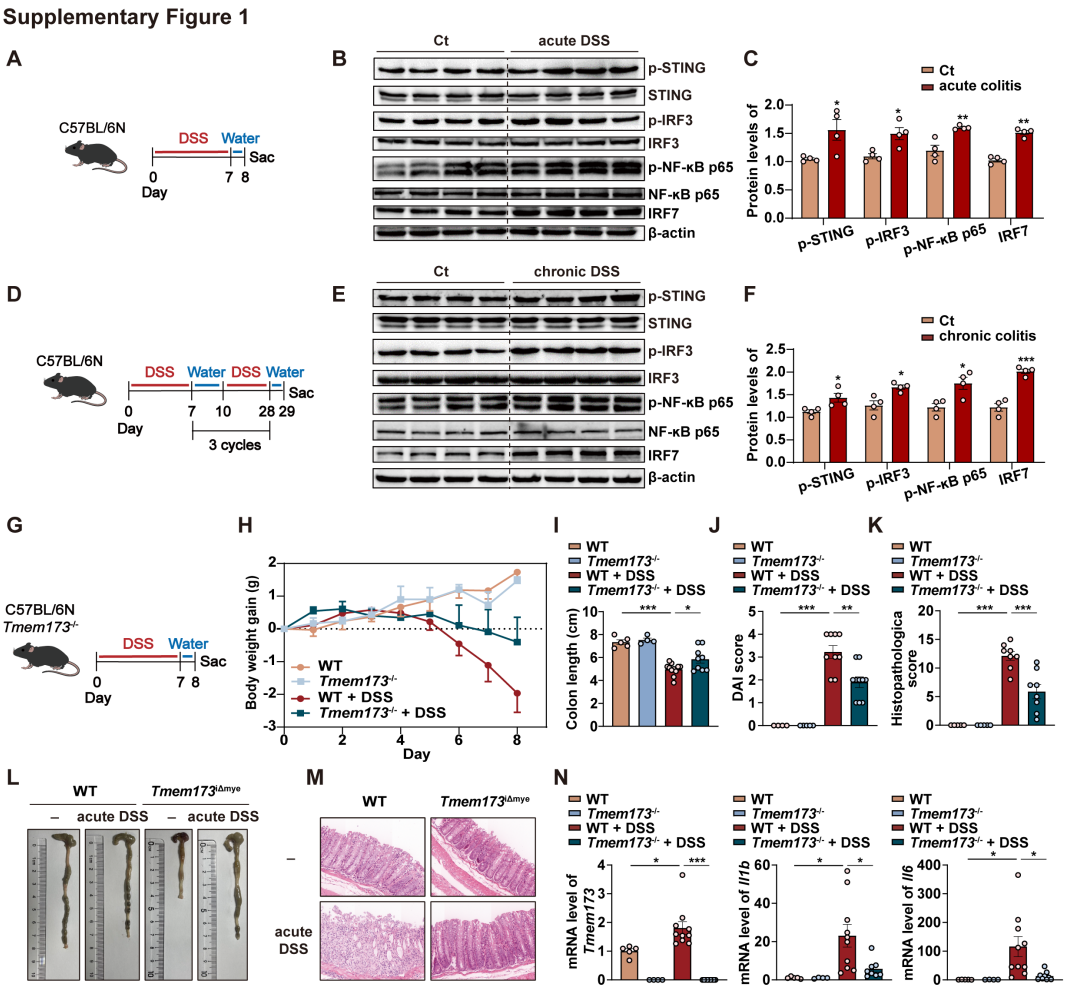

Supplementary Figure 1. (A-C) C57BL/6N mice were induced by acute DSS colitis. **(A)** Animal experimental design. **(B-C)** Representative images and quantitative analysis of immunoblotting detecting phosphorylation of STING, IRF3, and NF-κB p65 and protein level of IRF7 in colon. **(D-F)** C57BL/6N mice were induced by chronic DSS colitis. **(D)** Animal experimental design. **(E-F)** Representative images and quantitative analysis of immunoblotting detecting phosphorylation of STING, IRF3, and NF-κB p65 and protein level of IRF7 in colon. **(G-N)** C57BL/6N mice and *Tmem173*$^{-/-}$ mice were induced by acute DSS colitis. **(G)** Animal experimental design. **(H)** Body weight gain. **(I)** Colon length. **(J)** DAI score. **(K)** Histopathological score. **(L)** Representative colon pictures. **(M)** Representative H&E staining of colonic sections. **(N)** Relative mRNA levels of *Tmem173*, *Il1b*, *Il6* in colon. Scale bars, 100 μm. Values represent the mean ± S.E.M. of at least four samples in each group. Statistical significance: *p < 0.05, **p < 0.01, ***p < 0.001.

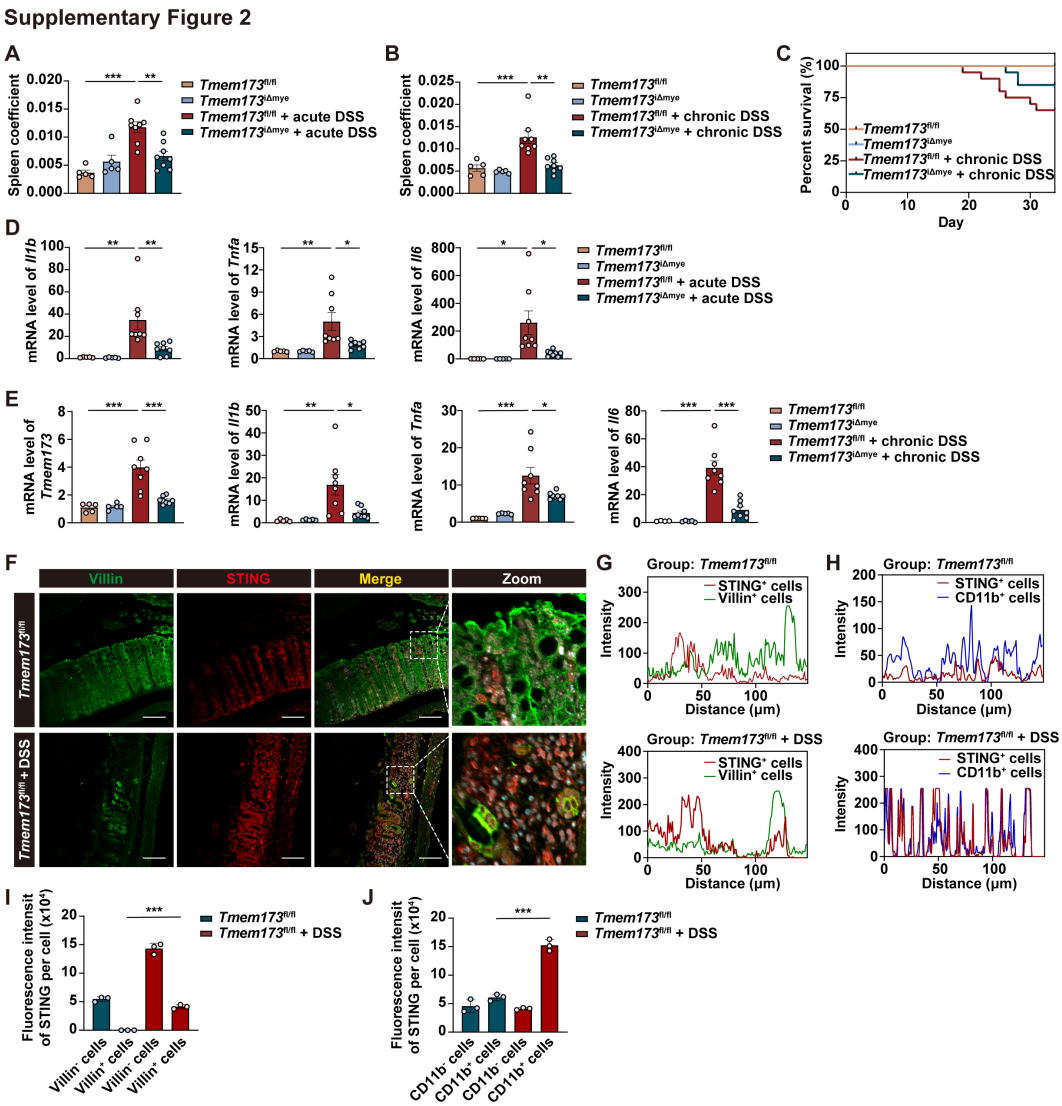

148

149 **Supplementary Figure 2. (A)** Spleen coefficient in acute colitis. **(B)** Spleen coefficient
150 in chronic colitis. **(C)** Survival rate in chronic colitis. **(D)** Relative mRNA levels of *Il1b*,
151 *Tnfa*, *Il6* in colon in acute colitis model. **(E)** Relative mRNA levels of *Tmem173*, *Il1b*,
152 *Tnfa*, *Il6* in colon in chronic model. **(F)** Representative immunofluorescent co-staining
153 of Villin and STING **(G)** The co-localization of Villin and STING in *Tmem173*$^{fl/fl}$ group
154 and *Tmem173*$^{fl/fl}$ +DSS group. **(H)** The co-localization of CD11b and STING in
155 *Tmem173*$^{fl/fl}$ group and *Tmem173*$^{fl/fl}$ +DSS group. **(I)** Mean fluorescence intensity of
156 STING in Villin^{-} and Villin^{+} cells in *Tmem173*$^{fl/fl}$ group and *Tmem173*$^{fl/fl}$ +DSS group. **(J)**
157 Mean fluorescence intensity of STING in CD11b^{-} and CD11b^{+} cells in *Tmem173*$^{fl/fl}$
158 group and *Tmem173*$^{fl/fl}$ +DSS group. Values represent the mean ± S.E.M. of at least
159 five mice in each group. Statistical significance: *p < 0.05, **p < 0.01, ***p < 0.001.

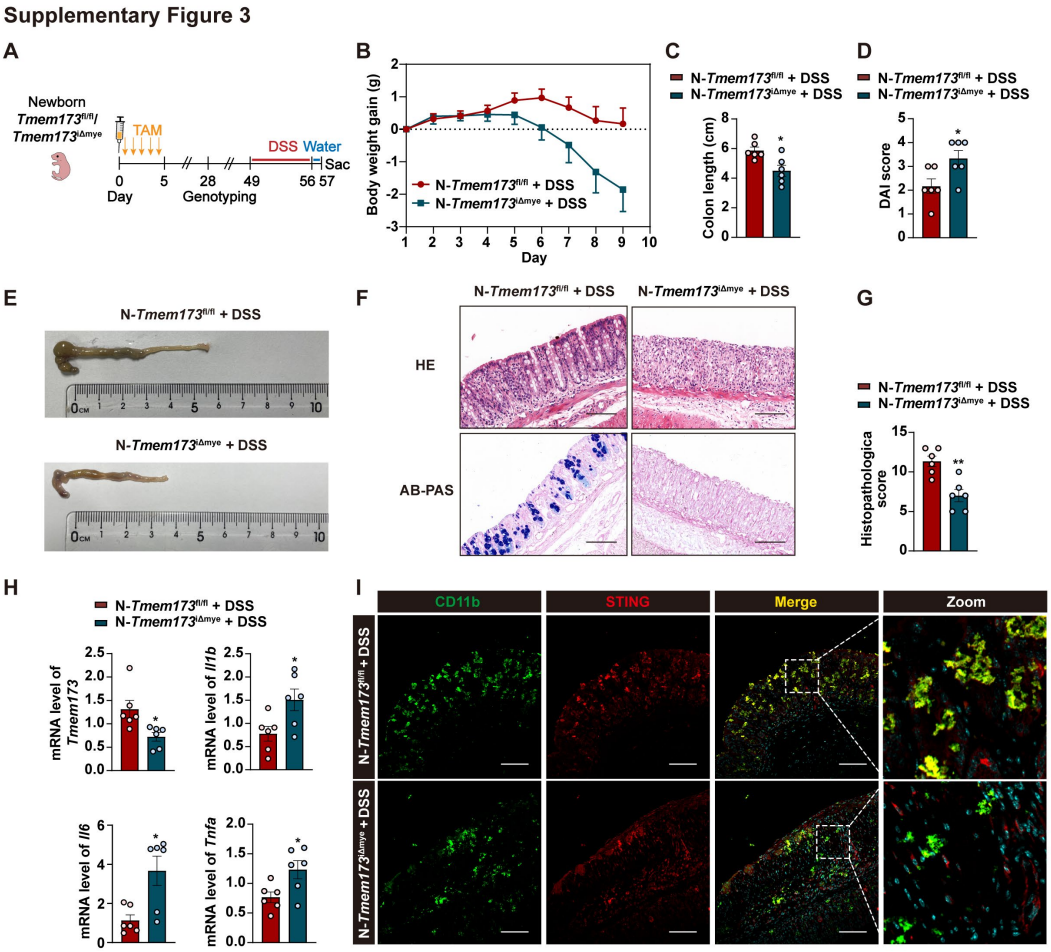

Supplementary Figure 3. Newborn *Tmem173*$^{fl/fl}$ mice and *Tmem173*$^{i\Delta mye}$ mice were induced by acute DSS colitis after TAM induction. **(A)** Animal experimental design. **(B)** Body weight gain. **(C)** Colon length. **(D)** DAI score. **(E)** Representative colon pictures. **(F)** Representative H&E and AB-PAS staining of colonic sections. **(G)** Histopathological score. **(H)** Relative mRNA levels of *Tmem173*, *Il1b*, *Il6* and *Tnfa* in colon. **(I)** Representative immunofluorescence co-staining of CD11b and STING of colonic sections. Scale bars, 100 μm. Values represent the mean ± S.E.M. of at least six mice in each group. Statistical significance: *p < 0.05, **p < 0.01.

Supplementary Figure 4

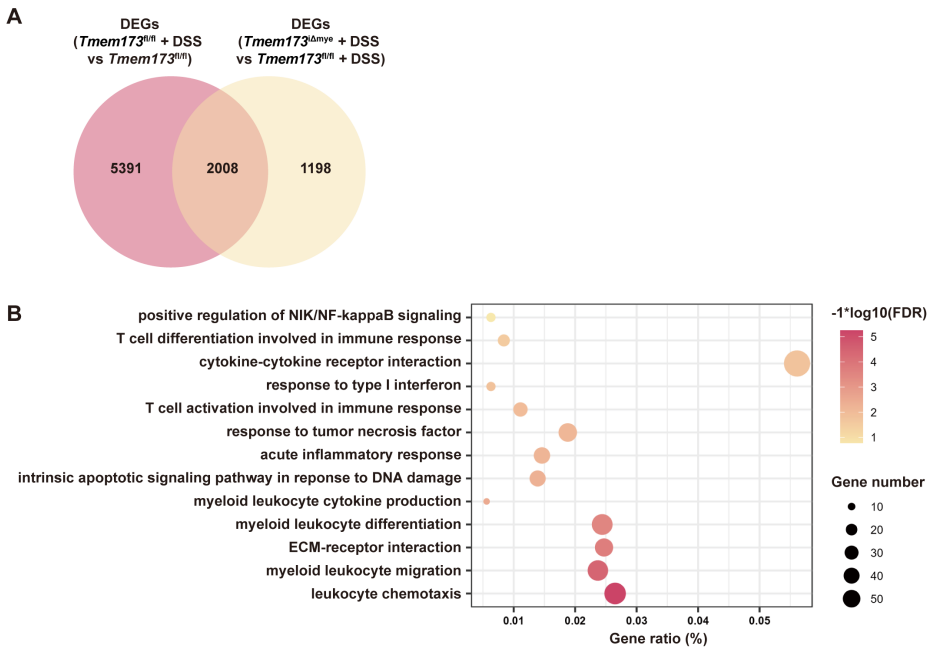

Supplementary Figure 4. (A) The overlap DEGs between *Tmem173*$^{fl/fl}$ + DSS vs. *Tmem173*$^{fl/fl}$ and *Tmem173*$^{i\Delta mye}$ + DSS vs. *Tmem173*$^{fl/fl}$ + DSS as indicated by Venn diagram. **(B)** Various inflammation-related pathways obtained by GO and KEGG enrichment analysis as indicated by bubble plot.

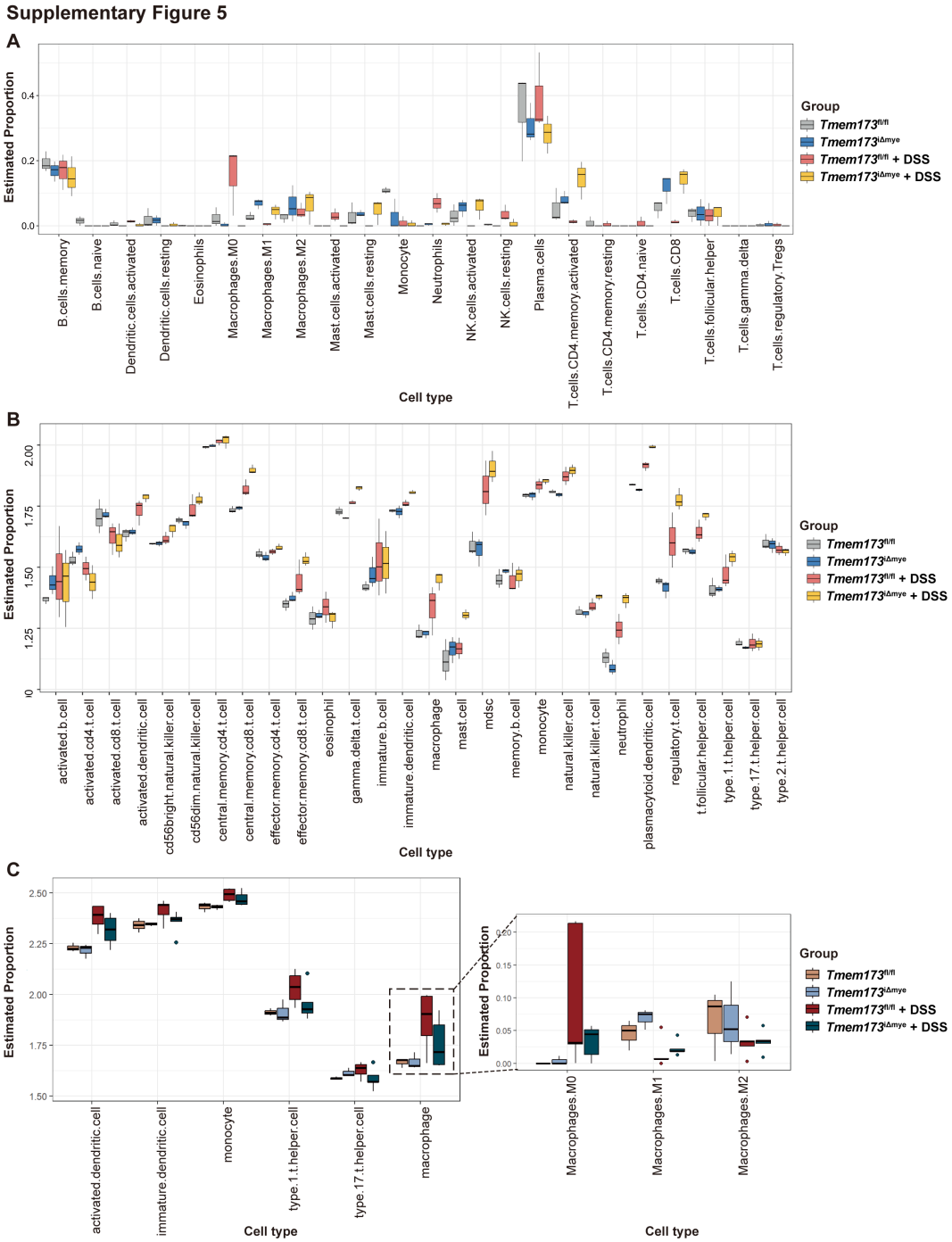

Supplementary Figure 5. (A) The immune cell infiltration analysis by CIBERSORT tool. **(B)** The immune cell infiltration analysis by ssGSEA tool. **(C)** The immune cell infiltration analysis by CIBERSORT tool and ssGSEA tool.

Supplementary Figure 6

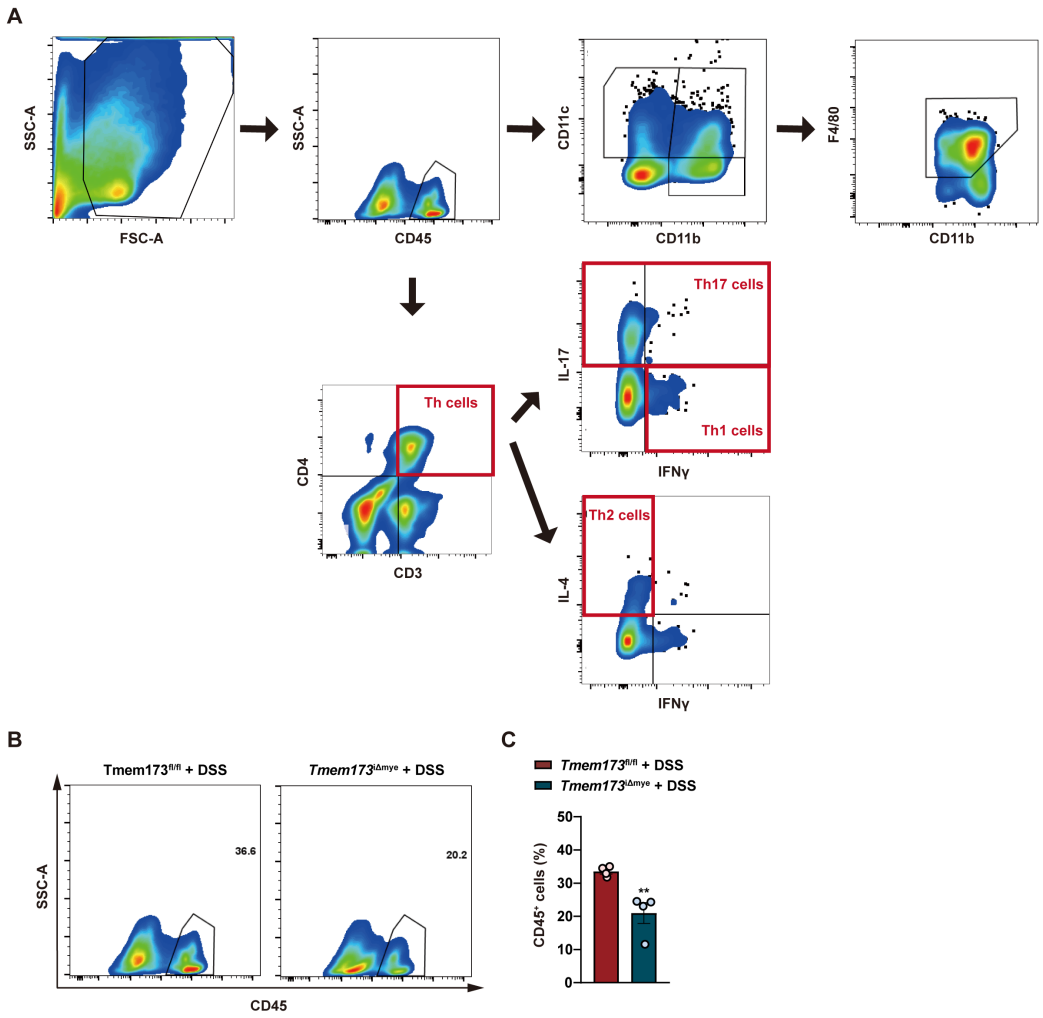

Supplementary Figure 6. (A) Sorting flow chart of flow cytometry for characterization of innate immune cells and adaptive immune cells. **(B-C)** Representative flow cytometry results and quantitative analysis of $CD45^+$ cells in the colonic lamina propria.

Supplementary Figure 7

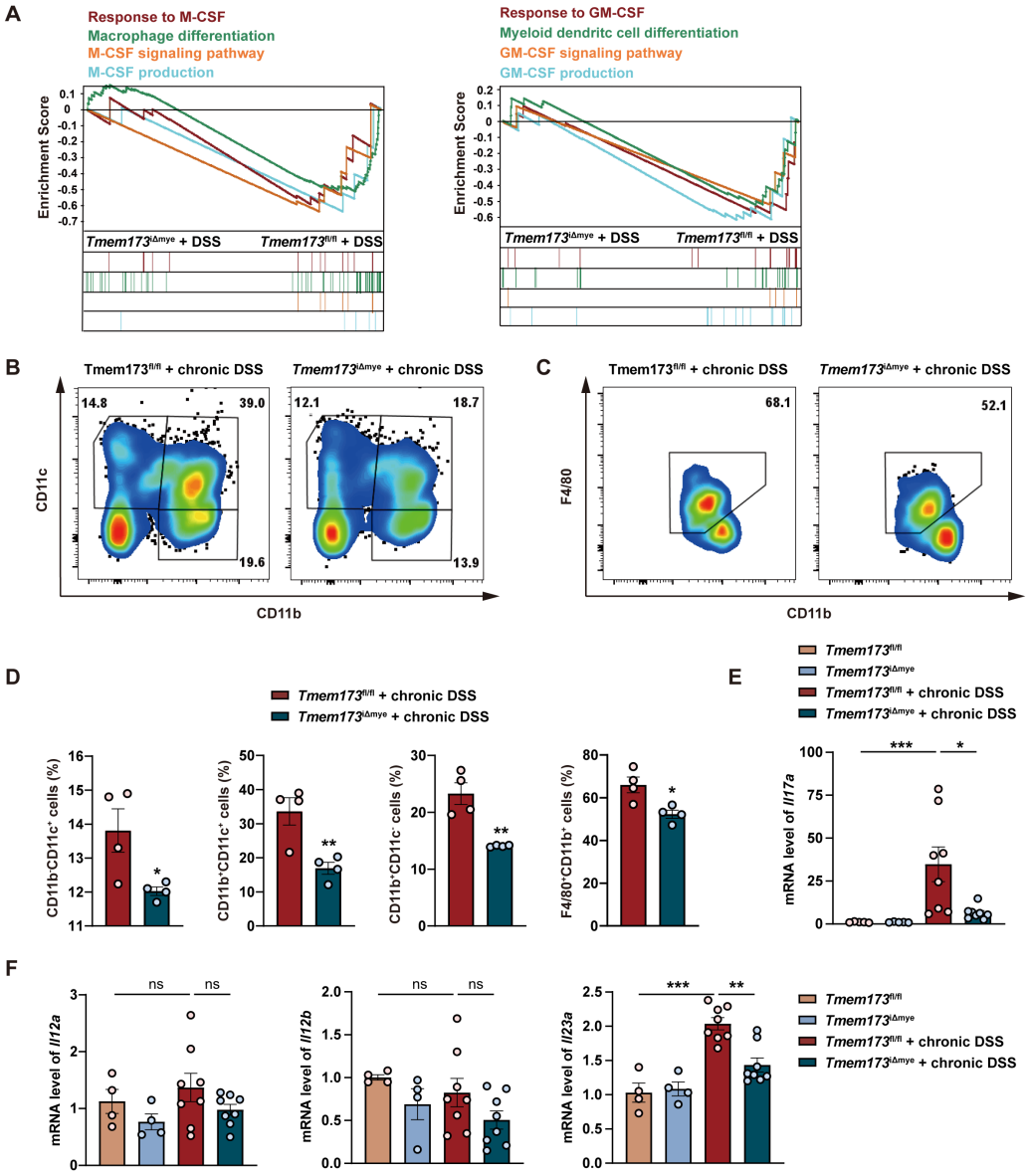

Supplementary Figure 7. (A) GSEA analysis of pathways related to macrophage and DC differentiation in *Tmem173*$^{i\Delta mye}$ + DSS *vs* *Tmem173*$^{fl/fl}$ + DSS. **(B-D)** Representative flow cytometry results and quantitative analysis of CD11b^{-}CD11c^{+} DCs, CD11b^{+}CD11c^{+} DCs, CD11b^{+}CD11c^{-} monocytes and F4/80^{+}CD11b^{+} macrophages in the colonic lamina propria in chronic DSS colitis model. **(E)** Relative mRNA levels of *Il17a* in colon in chronic DSS colitis model. **(F)** Relative mRNA levels of *Il12a*, *Il12b*, *Il23a* in colon in chronic DSS colitis model.

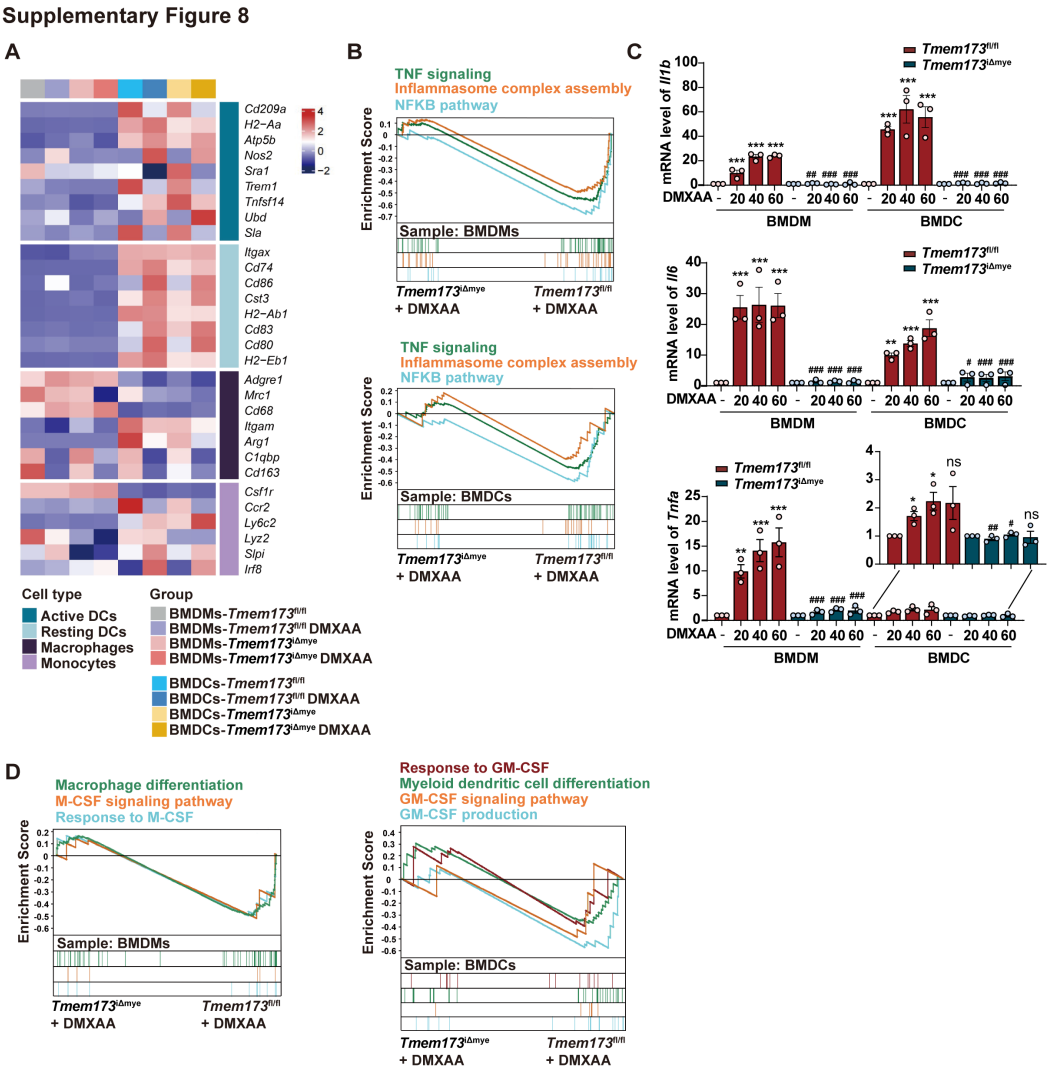

Supplementary Figure 8. (A) Gene maker expressions of active DCs, resting DCs, macrophage and monocyte in WT or STING KO BMDMs and BMDCs with or without DMXAA as indicated by heatmap. **(B)** GSEA analysis of classic inflammatory pathways in *Tmem173*$^{i\Delta mye}$ + DMXAA *vs* *Tmem173*$^{fl/fl}$ + DMXAA in BMDMs and BMDCs. **(C)** Relative mRNA levels of *Il1b*, *Il6*, and *Tnfa* in BMDMs and BMDCs. **(D)** GSEA analysis of pathways related to macrophage differentiation in *Tmem173*$^{i\Delta mye}$ + DMXAA *vs* *Tmem173*$^{fl/fl}$ + DMXAA in BMDMs, and pathways related to DC differentiation in *Tmem173*$^{i\Delta mye}$ + DMXAA *vs* *Tmem173*$^{fl/fl}$ + DMXAA in BMDCs. Values represent the mean ± S.E.M. of at least three samples in each group. Statistical significance relative to vehicle control: ns, no significant, *p < 0.05, **p < 0.01, ***p < 0.001. Statistical

206 significance relative to *Tmem173*$^{fl/fl}$ + DMXAA group: ns, no significant, $^{\#}p < 0.5$, $^{\#\#}p <$

207 0.01, $^{\#\#\#}p < 0.001$.

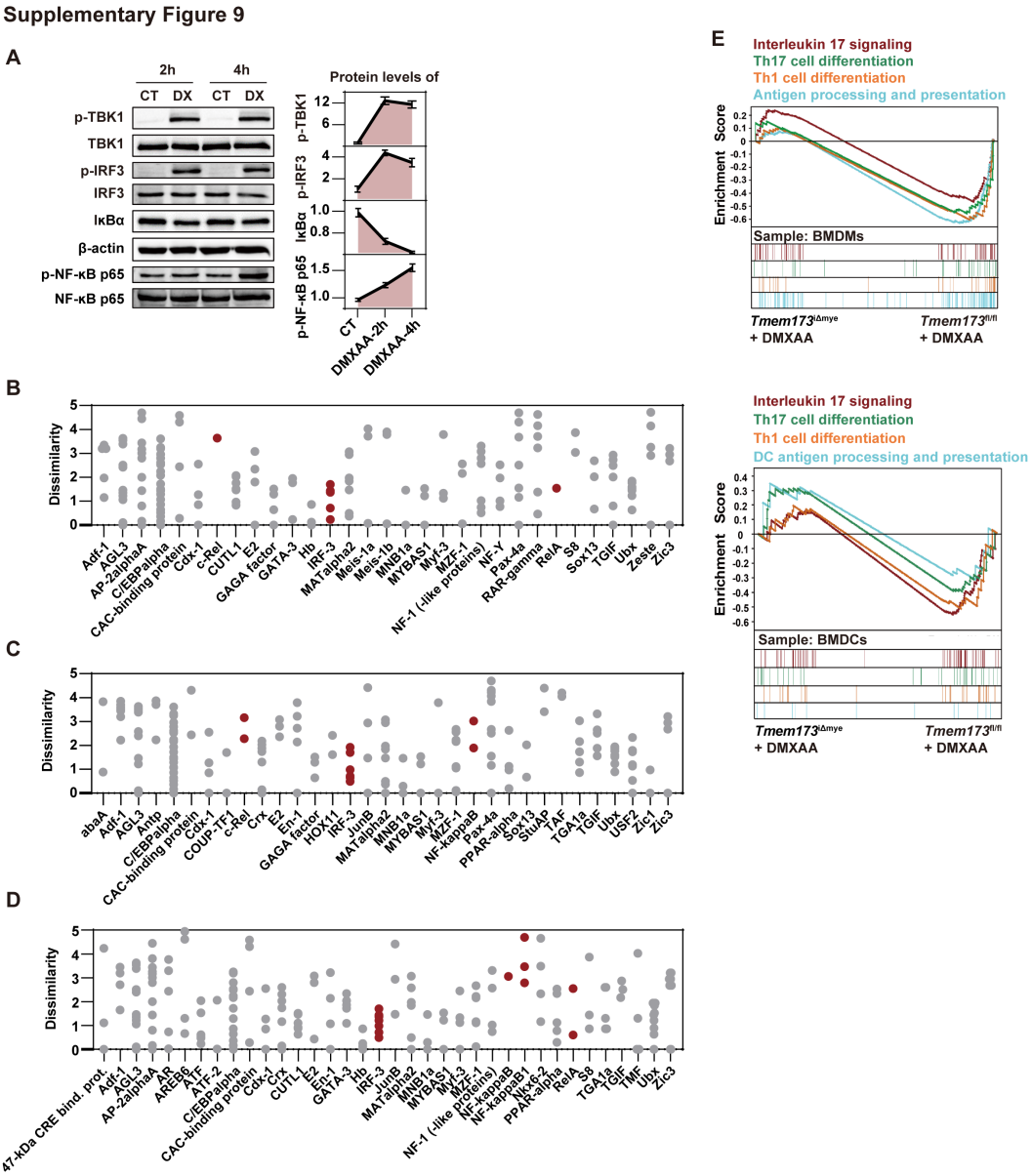

Supplementary Figure 9. (A) WT BMDCs were stimulated by vehicle control or DMXAA for 2 h and 4 h before cells were lysed for immunoblotting. Representative images and quantitative analysis of immunoblotting detecting phosphorylation of TBK1, IRF3, and NF-κB p65 and protein level of IκBα in WT BMDCs. **(B-D)** The number and dissimilarity of predicted transcription factors on promoters of IL-12 family genes (dissimilarity < 5). **(E)** GSEA analysis of pathways related to IL-17 signaling, Th1 and Th17 differentiation and antigen processing and presentation in *Tmem173*$^{i\Delta mye}$ + DMXAA *vs* *Tmem173*$^{fl/fl}$ + DMXAA in BMDMs and BMDCs.

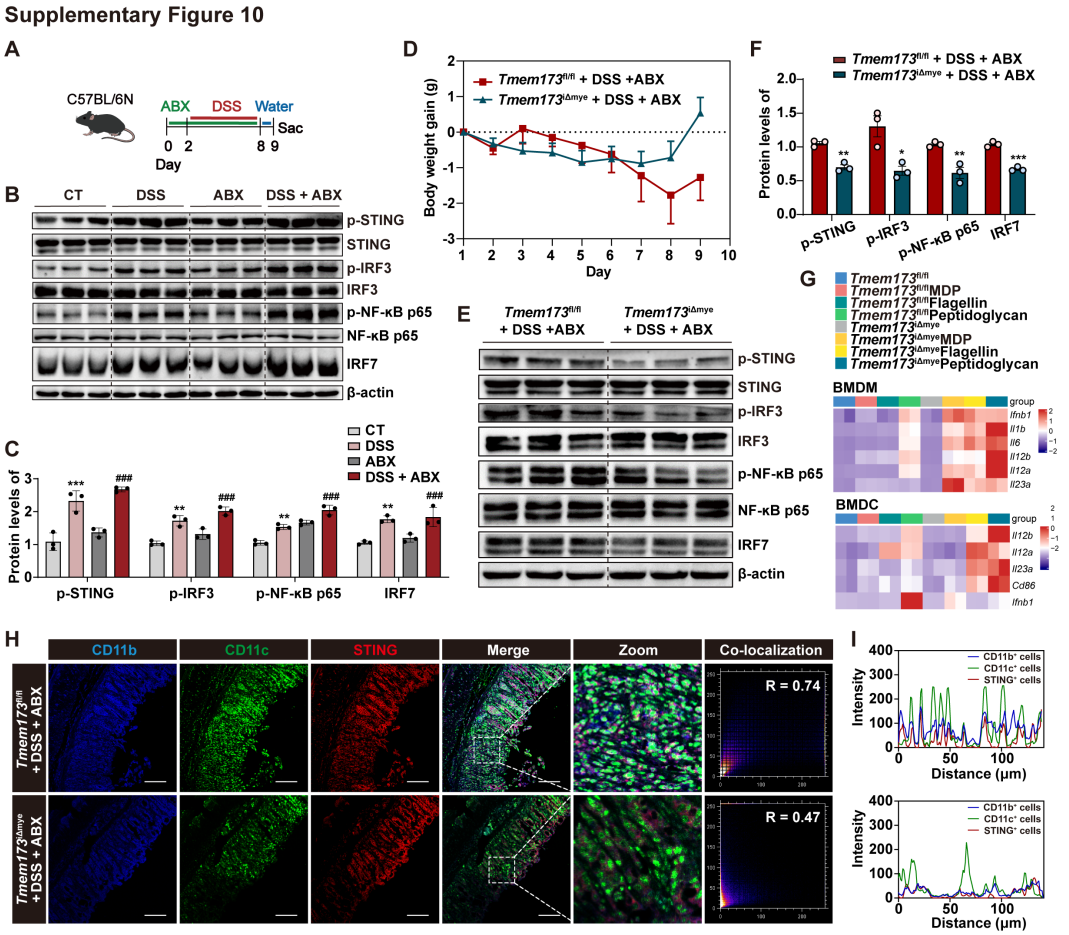

Supplementary Figure 10. (A-C) C57BL/6N mice were induced by acute DSS colitis and ABX. **(A)** Animal experimental design. **(B-C)** Representative images and quantitative analysis of immunoblotting detecting phosphorylation of STING, IRF3, and NF-κB p65 and protein level of IRF7 in colon. **(D-H)** *Tmem173*$^{fl/fl}$ mice and *Tmem173*$^{i\Delta mye}$ mice were treated by antibiotic cocktail (ABX) and then subjected to acute DSS administration. **(D)** Body weight gain. **(E-F)** Representative images and quantitative analysis of immunoblotting detecting the phosphorylation of STING, IRF3, and NF-κB p65 and the protein levels of IRF7 in the colon. **(G)** WT and STING KO BMDMs and BMDCs were treated with MDP, peptidoglycan, and flagellin for 8h. Relative mRNA levels of indicated genes are shown as a heatmap. **(H-I)** Representative immunofluorescent co-staining and quantitative analysis of CD11b, CD11c and STING of colonic sections. Scale bars, 100 μm. Values represent the mean ± S.E.M. of at least three samples in each group. Statistical significance relative to

vehicle control or *Tmem173*$^{fl/fl}$ + DSS +ABX group: *p < 0.05, **p < 0.01, ***p < 0.001; relative to ABX group: $^{\#}$p < 0.05, $^{\#\#}$p < 0.01, $^{\#\#\#}$p < 0.001.

Supplementary Figure 11

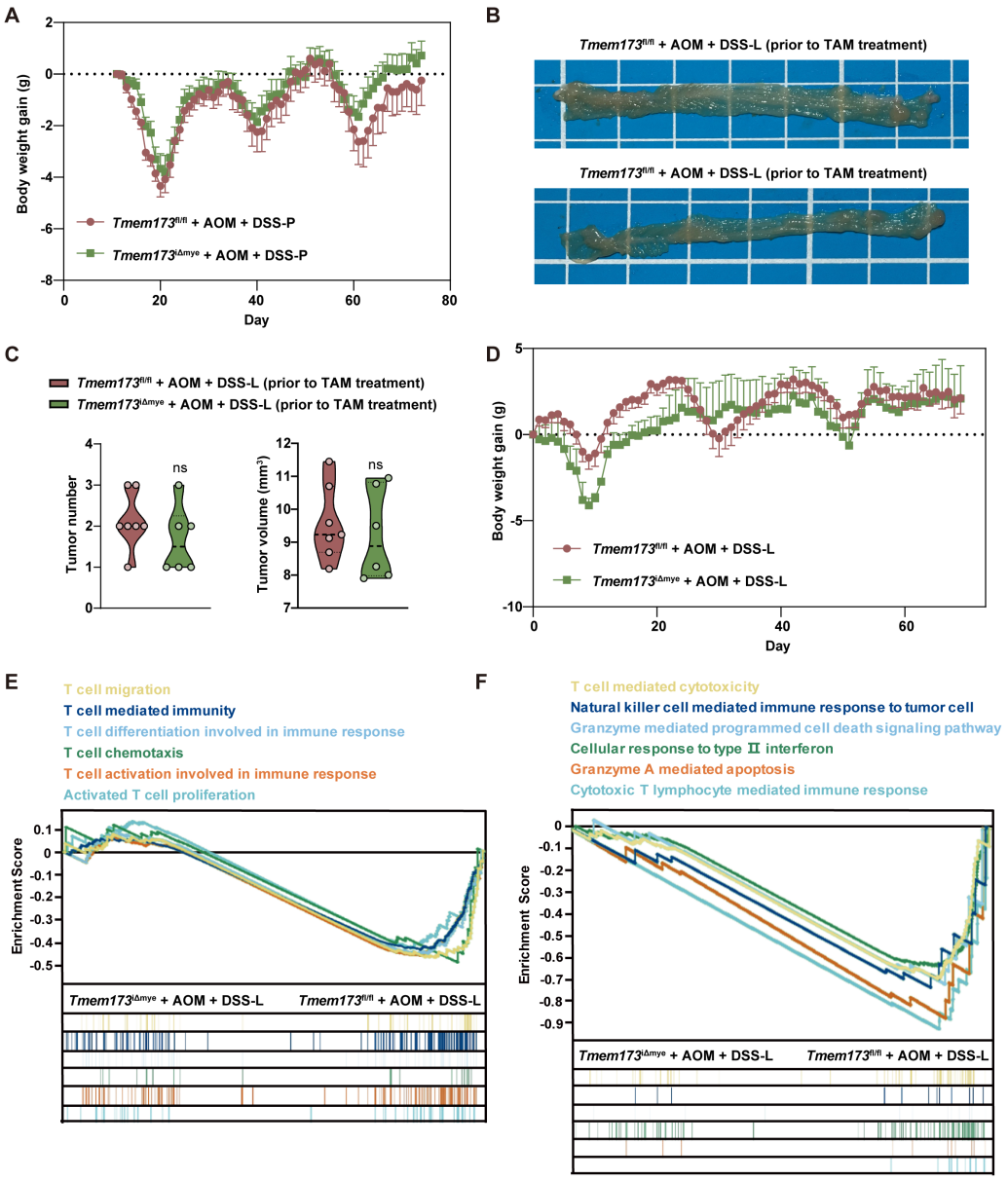

Supplementary Figure 11. (A) Body weight gain in AOM + DSS-P groups. **(B)** Representative pictures of colon samples and **(C)** the tumor number and volume in AOM + DSS-L groups before TAM induction from a preliminary experiment. **(D)** Body weight gain in AOM + DSS-L groups. **(E)** GSEA analysis of pathways related to T cell activity in *Tmem173*$^{i\Delta mye}$ + AOM + DSS-L *vs* *Tmem173*$^{fl/fl}$ + AOM + DSS-L in tumor tissues. **(F)** GSEA analysis of pathways related to tumor killing effects in *Tmem173*$^{i\Delta mye}$ + AOM + DSS-L *vs* *Tmem173*$^{fl/fl}$ + AOM + DSS-L in tumor tissues.

Supplementary Figure 12

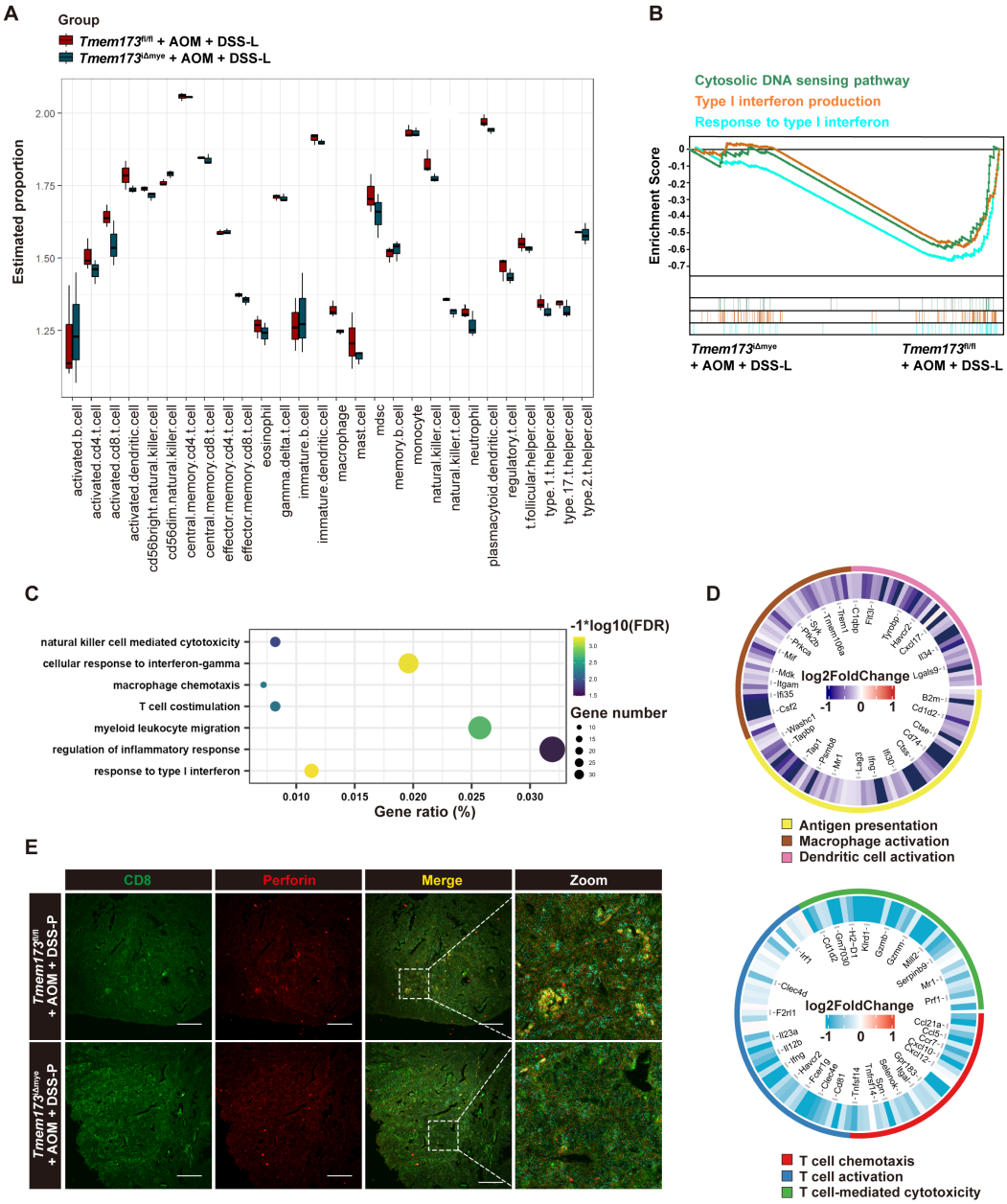

Supplementary Figure 12. (A) The immune cell infiltration analysis by ssGSEA tool based on RNA-seq data of tumor tissues. **(B)** GSEA analysis of pathways related to STING and type I IFNs in *Tmem173*$^{i\Delta mye}$ + AOM + DSS-L *vs* *Tmem173*$^{fl/fl}$ + AOM + DSS-L in tumor tissues. **(C)** Various inflammation-related pathways obtained by GO and KEGG enrichment analysis as indicated by bubble plot. **(D)** Log2FoldChange of gene expressions of innate immune and adaptive immune responses in *Tmem173*$^{i\Delta mye}$ + AOM + DSS-L *vs* *Tmem173*$^{fl/fl}$ + AOM + DSS-L in tumor tissues as indicated by

252 circular heatmap. **(E)** Representative immunofluorescence co-staining of CD8 and
253 Perforin of colonic sections. Scale bars, 100 μm.
254